Supplementary Information (SI) for Chemical Science.
This journal is © The Royal Society of Chemistry 2026

# Supplementary Information

## Unraveling the Positive Effect of Twisted Helicene Structure on Narrowband Electroluminescence

Cheng-Zhuo Du,[†a] Minqiang Mai,[†b] Pei-Han Gao,[a] Yi-Chao Zhao,[a] Xiang-Yu Gao,[a] Dongdong Zhang,*[b] Lian Duan,*[b] Chunming Cui[a] and Xiao-Ye Wang*[ac]

[a]State Key Laboratory of Elemento-Organic Chemistry, Frontiers Science Center for New Organic Matter, Haihe Laboratory of Sustainable Chemical Transformations, Academy for Advanced Interdisciplinary Studies, College of Chemistry, Nankai University, Tianjin, 300071, China. E-mail: xiaoye.wang@nankai.edu.cn

Homepage: http://wang.nankai.edu.cn

[b]Key Lab of Organic Optoelectronics and Molecular Engineering of Ministry of Education, Department of Chemistry, Tsinghua University, Beijing, 100084, China.

[c]Beijing National Laboratory for Molecular Sciences, Beijing, 100190, China.

[†]These authors contributed equally.

# Table of Contents

# 1. General Methods

Unless otherwise noted, reagents were commercially available and used as purchased without further purification. Chemicals were purchased from J&K Chemicals, Adamas-beta, Macklin Reagent, Energy Chemicals, Aladdin, leyan or Bide Pharmatech Ltd. All oxygen- or moisture-sensitive reactions were operated under an argon atmosphere according to the standard Schlenk method. Work-up and purification procedures were carried out with reagent-grade solvents under air. Thin layer chromatography (TLC) was performed on silica gel with GF254 indicator. All yields given refer to isolated yields. Nuclear magnetic resonance (NMR) spectra were recorded on Bruker AVANCE 400 spectrometers at 400 MHz ($^{1}$H NMR) and 100 MHz ($^{13}$C NMR). Chemical shifts ($\delta$) were reported in ppm. Signal splitting patterns were described as singlet (s), doublet (d), triplet (t), quartet (q), or multiplet (m) and coupling constants ($J$) were reported in Hz. $^{1}$H NMR chemical shifts were referenced to $CHCl_3$ (7.260 ppm), $CHDCl_2$ (5.320 ppm). $^{13}$C NMR chemical shifts were referenced to $CDCl_3$ (77.16 ppm), $CD_2Cl_2$ (54.00 ppm). High-resolution mass spectrometry (HRMS) was performed on Bruker Solarix scimax MRMS by matrix-assisted laser desorption/ionization (MALDI).

UV-vis absorption spectra were recorded on a PerkinElmer UV-vis Lambda 365 spectrophotometer. Fluorescence spectra were recorded on an Edinburgh FS5 Spectrofluorometer and the photoluminescence quantum yields (PLQYs) were measured by an integrating sphere. The phosphorescence spectra were recorded at 77 K in dilute toluene ($1\times10^{-5}$ M) after the solution was bubbled with nitrogen for 10 min on a Hitachi F-7000 Fluorescence Spectrometer. The transient photoluminescence spectra were collected on an Edinburgh FLS1000 Spectrofluorometer equipped with a R928P photomultiplier tube. Transient decay curves for prompt fluorescence were collected with a 442 nm picosecond pulsed LED (EPL450), while the delayed parts were collected with a μF2 micro-flash lamp.

Thermogravimetric analysis (TGA) was performed using a NETZSCH TG 209 analyzer at a heating rate of 10 °C min$^{-1}$ under a nitrogen atmosphere. The thermal decomposition temperatures ($T_d$) were determined by the recorded temperature at 5% weight loss. Differential scanning calorimetry (DSC) measurements were performed on NETZSCH DSC 204 instrument at a heating rate of 10 °C min$^{-1}$ under a nitrogen atmosphere. Cyclic voltammetry (CV) and differential pulse voltammetry (DPV) characterizations were carried out in anhydrous tetrahydrofuran (THF) containing 0.1 M $n$-$Bu_4NPF_6$ as supporting electrolyte (scan rate: 100 mV s$^{-1}$) under an argon atmosphere on a CHI 620E electrochemical analyzer. A three-electrode system was adopted with glassy carbon as the working electrode, platinum wire as the counter electrode, and Ag/AgCl as the reference electrode. The redox potentials were calibrated with ferrocene as an external standard.

## 2. Synthetic Procedures

7*H*-diphenanthro[9,10-*c*:9',10'-*g*]carbazole[1] (**7H**) and 9-(2-bromo-3-fluorophenyl)-3,6-di-*tert*-butyl-9*H*-carbazole[2] (**1**) were synthesized according to the reported procedure.

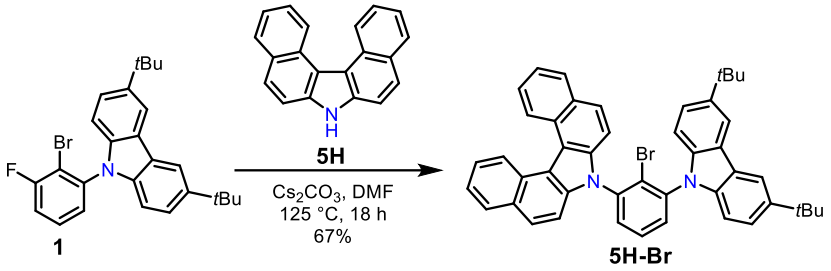


**7-(2-bromo-3-(3,6-di-*tert*-butyl-9*H*-carbazol-9-yl)phenyl)-7*H*-dibenzo[*c,g*]carbazole (5H-Br).** To a Schlenk flask under argon was added **1** (3.64 g, 8.05 mmol), 7*H*-dibenzo[*c,g*]carbazole (**5H**) (Cat No. 1149505, Leyan, Shanghai, China) (2.87 g, 10.7 mmol), $Cs_2CO_3$ (4.65 g, 14.3 mmol), and *N*,*N*-dimethylformamide (DMF) (120 mL). The reaction mixture was stirred at 125 °C for 18 h. After cooling down to room temperature, the mixture was poured into water and the residue was purified by column chromatography over silica gel (petroleum ether/$CH_2Cl_2$ = 5:1) and further recrystallization from $CH_2Cl_2$/MeOH to afford 3.80 g (yield: 67%) of **5H-Br** as a white solid. $^1$H NMR (400 MHz, $CDCl_3$, 297 K, ppm) $\delta$ 9.29 (d, $J$ = 8.4 Hz, 2H), 8.16 (d, $J$ = 1.6 Hz, 2H), 8.07 (d, $J$ = 8.8 Hz, 2H), 7.93 (d, $J$ = 8.8 Hz, 2H), 7.82 – 7.71 (m, 5H), 7.58 – 7.50 (m, 4H), 7.43 (d, $J$ = 8.8 Hz, 2H), 7.16 (d, $J$ = 8.8 Hz, 2H), 1.47 (s, 18H). $^{13}$C NMR (100 MHz, $CDCl_3$, 297 K, ppm) $\delta$ 143.39, 139.97, 139.23, 138.73, 137.89, 131.87, 131.36, 130.45, 129.57, 129.39, 129.28, 127.34, 126.41, 125.79, 125.53, 123.97, 123.75, 123.57, 118.06, 116.64, 111.66, 109.52, 34.92, 32.15. HRMS (MALDI) *m/z*: Calcd. for $C_{46}H_{39}BrN_2^+$: 698.2291; Found: 698.2294 $[M]^+$.

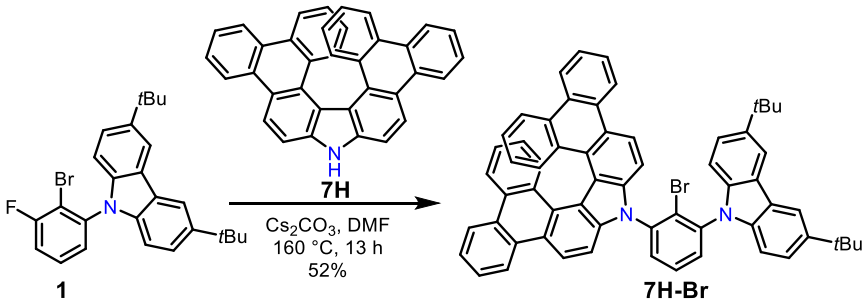


**7-(2-bromo-3-(3,6-di-*tert*-butyl-9H-carbazol-9-yl)phenyl)-7H-diphenanthro[9,10-*c*:9',10'-*g*]carbazole (7H-Br).** To a Schlenk flask under argon was added **1** (1.66 g, 3.67 mmol), 7*H*-diphenanthro[9,10-*c*:9',10'-*g*]carbazole (**7H**) (2.57 g, 5.50 mmol), $Cs_2CO_3$ (5.97 g, 18.3 mmol), and DMF (60 mL). The reaction mixture was stirred at 160 °C for 13 h. After cooling down to room temperature, the mixture was poured into water and the residue was purified by column chromatography over silica gel (eluent: petroleum ether/$CH_2Cl_2$ = 10:1) and further recrystallization from $CH_2Cl_2$/MeOH to afford 1.72 g (yield: 52%) of **7H-Br** as a light-yellow solid. $^1$H NMR (400 MHz, $CD_2Cl_2$, 297 K, ppm) $\delta$ 8.90 – 8.83 (m, 2H), 8.80 – 8.70 (m, 4H), 8.48 (t, $J$ = 8.0 Hz,

2H), 8.23 – 8.18 (m, 2H), 8.08 – 7.84 (m, 6H), 7.78 – 7.67 (m, 5H), 7.65 – 7.53 (m, 3H), 7.31 – 7.20 (m, 3H), 6.42 – 6.34 (m, 2H). 1.51 – 1.46 (m, 18H). $^{13}$C NMR (100 MHz, $CDCl_3$, 297 K, ppm) $\delta$ 143.66, 143.46, 143.44, 141.24, 140.87, 140.21, 139.34, 139.27, 138.86, 132.02, 131.64, 130.84, 130.64, 129.78, 129.55, 129.52, 128.73, 128.68, 128.44, 128.16, 127.86, 127.28, 127.25, 127.11, 127.09, 126.58, 126.18, 126.14, 124.98, 124.89, 124.67, 124.03, 124.02, 123.76, 123.69, 123.68, 123.61, 123.42, 123.38, 121.96, 121.89, 121.87, 118.98, 118.86, 118.79, 116.72, 116.67, 110.38, 110.26, 109.64, 109.56, 109.33, 34.97, 34.94, 32.20, 32.16. HRMS (MALDI) *m/z*: Calcd. for $C_{62}H_{47}BrN_2^+$: 898.2917; Found: 898.2936 $[M]^+$.

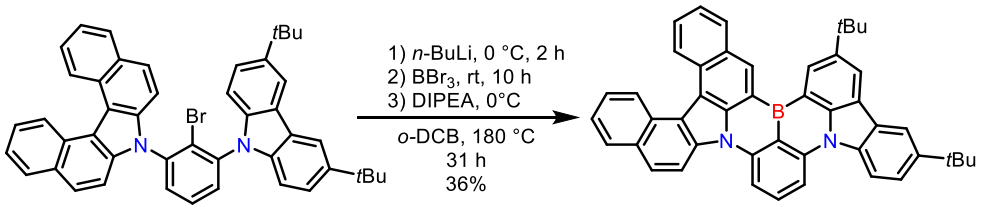


**5H-Br** **BN-5H**

**BN-5H.** To a solution of **5H-Br** (3.80 g, 5.43 mmol) in 1,2-dichlorobenzene (*o*-DCB) (54 mL) was slowly added *n*-BuLi (10.8 mmol, 1.6 M in hexane) at 0 °C under an argon atmosphere. After stirring for 2 h at 0 °C, $BBr_3$ (10.8 mmol, 1.0 M in heptane) was slowly added to the mixture, which was then stirred at room temperature for 10 h. The low boiling point solvents were removed under reduced pressure and *N*,*N*-diisopropylethylamine (DIPEA) (1.8 mL) was added at 0 °C. The mixture was stirred at 180 °C for 31 h. After cooling down to room temperature, the solvent was removed under reduced pressure; the residue was purified by column chromatography over silica gel (eluent: petroleum ether/$CH_2Cl_2$ = 5:1) and further recrystallization from $CH_2Cl_2$/MeOH to afford 1.23 g (yield: 36%) of **BN-5H** as a yellow solid. $^1$H NMR (400 MHz, $CD_2Cl_2$, 297 K, ppm) $\delta$ 9.49 (s, 1H), 9.26 – 9.19 (m, 3H), 8.77 (d, $J$ = 9.2 Hz, 1H), 8.59 (d, $J$ = 2.0 Hz, 1H), 8.45 – 8.36 (m, 4H), 8.34 (d, $J$ = 2.0 Hz, 1H), 8.12 (d, $J$ = 8.0 Hz, 1H), 8.09 – 8.03 (m, 2H), 7.84 – 7.78 (m, 1H), 7.78 – 7.59 (m, 4H), 1.72 (s, 9H), 1.55 (s, 9H). $^{13}$C NMR (100 MHz, $CD_2Cl_2$, 297 K, ppm) $\delta$ 146.33, 145.66, 144.39, 142.50, 141.87, 139.89, 138.78, 137.15, 137.09, 133.98, 131.47, 131.30, 131.09, 130.77, 130.22, 129.35, 129.17, 127.73, 127.55, 127.01, 126.52, 126.07, 125.85, 125.13, 124.84, 124.49, 124.36, 122.19, 122.11, 118.03, 117.63, 115.23, 114.74, 110.30, 110.10, 35.73, 35.29, 32.53, 32.11 (The aromatic carbons *ipso* to the boron atoms were not observed due to quadrupolar relaxation). HRMS (MALDI) *m/z*: Calcd. for $C_{46}H_{37}BN_2^+$: 628.3044; Found: 628.3048 $[M]^+$.

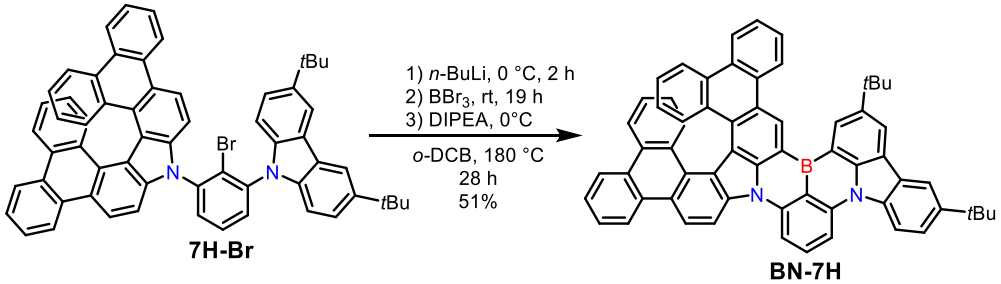


**7H-Br** **BN-7H**

**BN-7H.** To a solution of **7H-Br** (4.97 g, 5.52 mmol) in *o*-DCB (55 mL) was slowly

added *n*-BuLi (16.6 mmol, 2.4 M in hexane) at 0 °C under an argon atmosphere. After stirring for 2 h at 0 °C, $BBr_3$ (16.6 mmol, 1.0 M in heptane) was slowly added to the mixture, which was then stirred at room temperature for 19 h. The low boiling point solvents were removed under reduced pressure and DIPEA (1.8 mL) was added at 0 °C. The mixture was stirred at 180 °C for 28 h. After cooling down to room temperature, the solvent was removed under reduced pressure; the residue was purified by column chromatography over silica gel (eluent: petroleum ether/$CH_2Cl_2$ = 5:1) and further recrystallization from $CH_2Cl_2$/MeOH to afford 2.32 g (yield: 51%) of **BN-7H** as an orange solid. $^1$H NMR (400 MHz, $CD_2Cl_2$, 297 K, ppm) $\delta$ 10.03 (s, 1H), 9.03 (d, $J$ = 1.6 Hz, 1H), 8.84 (d, $J$ = 8.0 Hz, 1H), 8.61 – 8.53 (m, 2H), 8.48 – 8.44 (m, 1H), 8.42 (d, $J$ = 1.6 Hz, 1H), 8.37 – 8.31 (m, 4H), 8.20 (d, $J$ = 2.4 Hz, 1H), 8.10 (d, $J$ = 8.8 Hz, 1H), 7.98 (t, $J$ = 7.6 Hz, 2H), 7.77 – 7.72 (m, 2H), 7.68 – 7.63 (m, 1H), 7.61 – 7.50 (m, 5H), 7.19 – 7.12 (m, 2H), 6.26 – 6.20 (m, 2H), 1.69 (s, 9H), 1.55 (s, 9H). $^{13}$C NMR (100 MHz, $CD_2Cl_2$, 297 K, ppm) $\delta$ 145.88, 145.16, 144.09, 143.65, 142.59, 141.90, 140.21, 138.70, 133.33, 131.41, 130.70, 130.69, 130.57, 130.52, 130.04, 129.94, 129.84, 129.36, 129.33, 129.27, 128.17, 127.96, 127.86, 127.77, 127.60, 127.56, 127.46, 126.84, 125.91, 125.75, 125.16, 125.11, 124.96, 124.34, 124.08, 124.03, 123.78, 123.50, 123.25, 122.43, 122.36, 122.27, 121.74, 121.55, 121.25, 118.94, 117.85, 114.74, 114.16, 109.64, 109.57, 35.65, 35.24, 32.51, 32.16 (The aromatic carbons *ipso* to the boron atoms were not observed due to quadrupolar relaxation). HRMS (MALDI) *m/z*: Calcd. for $C_{62}H_{45}BN_2^+$: 828.3670; Found: 828.3675 $[M]^+$.

## 3. Thermal Properties

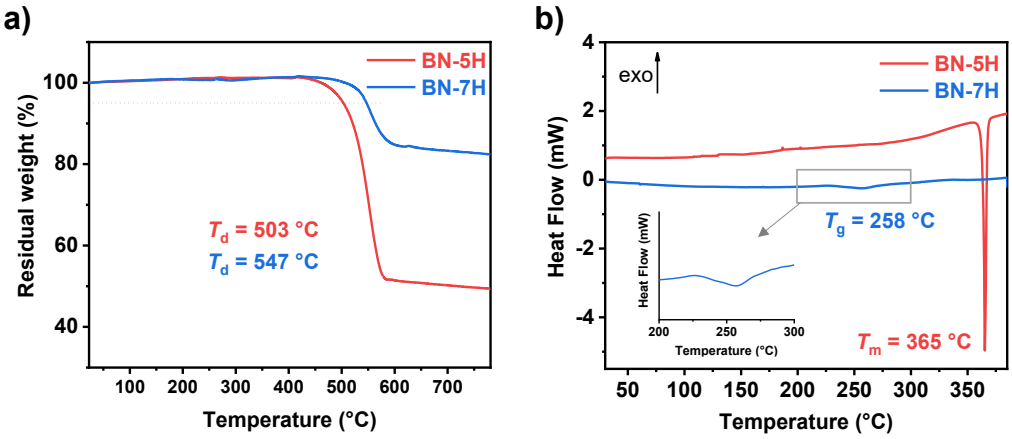


**Figure S1**. (a) Thermogravimetric analysis (TGA) and (b) differential scanning calorimetry (DSC) curves of BN-5H and BN-7H at a heating rate of 10 °C $min^{-1}$ under a nitrogen atmosphere. Decomposition temperature ($T_d$): 5% weight loss. Glass transition temperatures: $T_g$. Melting temperature: $T_m$. The $T_g$ of BN-7H are observed at 258 °C, while no $T_g$ was observed for BN-5H before its melting temperature ($T_m$) of 365 °C.

## 4. Photophysical and Electrochemical Properties

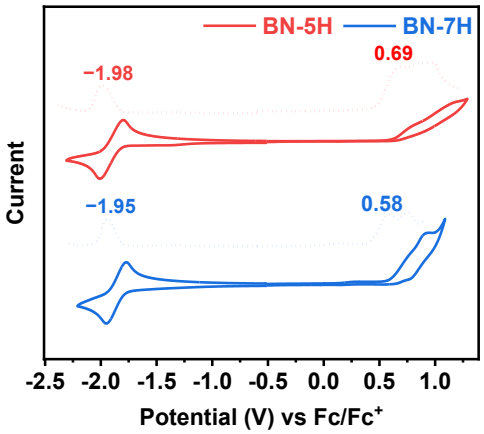


**Figure S2.** Cyclic voltammograms (CV) (solid lines) and differential pulse voltammograms (DPV) (dotted lines) of BN-5H and BN-7H in THF (1 mM) with 0.1 M *n*-$Bu_4NPF_6$ as supporting electrolyte and ferrocene as an external standard. Scan rate: 100 mV $s^{-1}$.

**Table S1**. Summary of the electrochemical properties of BN-5H and BN-7H.

| Compound | $HOMO^{CV}$ (eV) | $LUMO^{CV}$ (eV) | $E_g^{CV}$ (eV) | $HOMO^{DPV}$ (eV) | $LUMO^{DPV}$ (eV) | $E_g^{DPV}$ (eV) |
|---|---|---|---|---|---|---|
| BN-5H | –5.42 | –2.97 | 2.45 | –5.49 | –2.82 | 2.67 |
| BN-7H | –5.40 | –3.01 | 2.39 | –5.38 | –2.85 | 2.53 |

The $HOMO^{CV}$ and $LUMO^{CV}$ energy levels are calculated according to the equations HOMO = −(4.80 + $E_{ox}^{onset}$) and LUMO = −(4.80 + $E_{red}^{onset}$), where $E_{ox}^{onset}$ and $E_{red}^{onset}$ are the onset potentials of the first oxidative and reductive waves on CV curves, respectively. $E_g^{CV}$ is calculated according to the equation $E_g^{CV} = LUMO^{CV}–HOMO^{CV}$. The $HOMO^{DPV}$ and $LUMO^{DPV}$ energy levels are calculated according to the first oxidative and reductive peak potentials on DPV curves, respectively. $E_g^{DPV}$ is calculated according to the equation $E_g^{DPV} = LUMO^{DPV}–HOMO^{DPV}$.

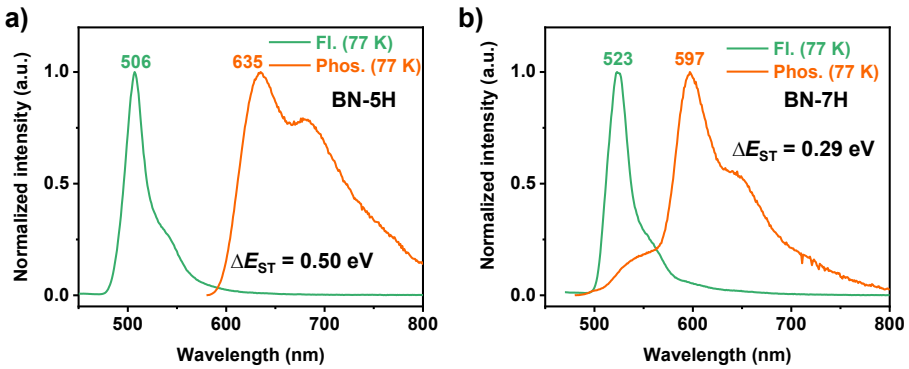


**Figure S3.** Normalized fluorescence (Fl.) and phosphorescence (Phos.) spectra of (a) BN-5H and (b) BN-7H in $1\times10^{-5}$ M toluene solutions at 77 K. Excited-state energy levels were estimated using the fluorescence and phosphorescence peak maxima.

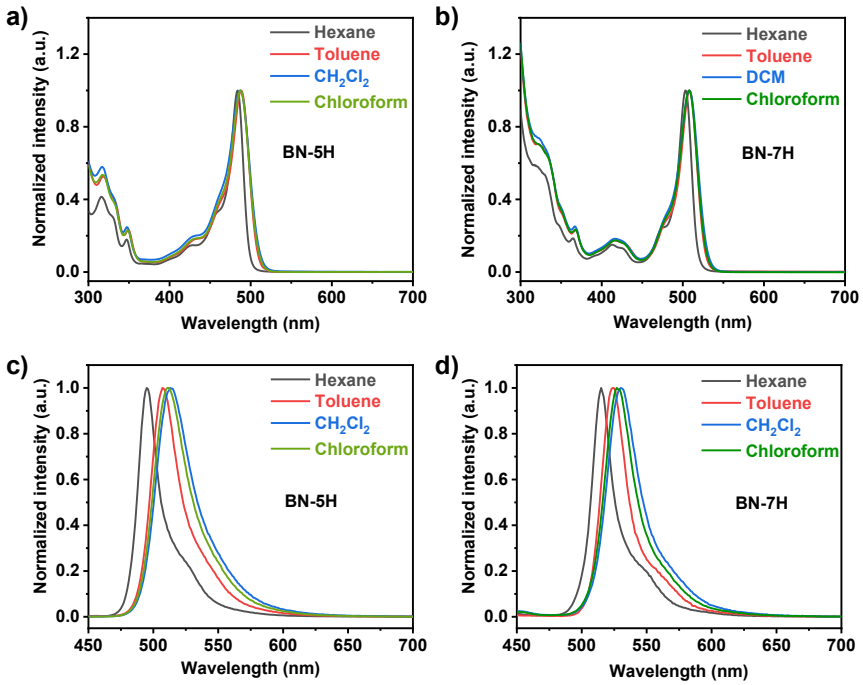


**Figure S4.** (a,b) Normalized absorption spectra and (c,d) fluorescence spectra of BN-5H and BN-7H in different solvents ($1\times10^{-5}$ M).

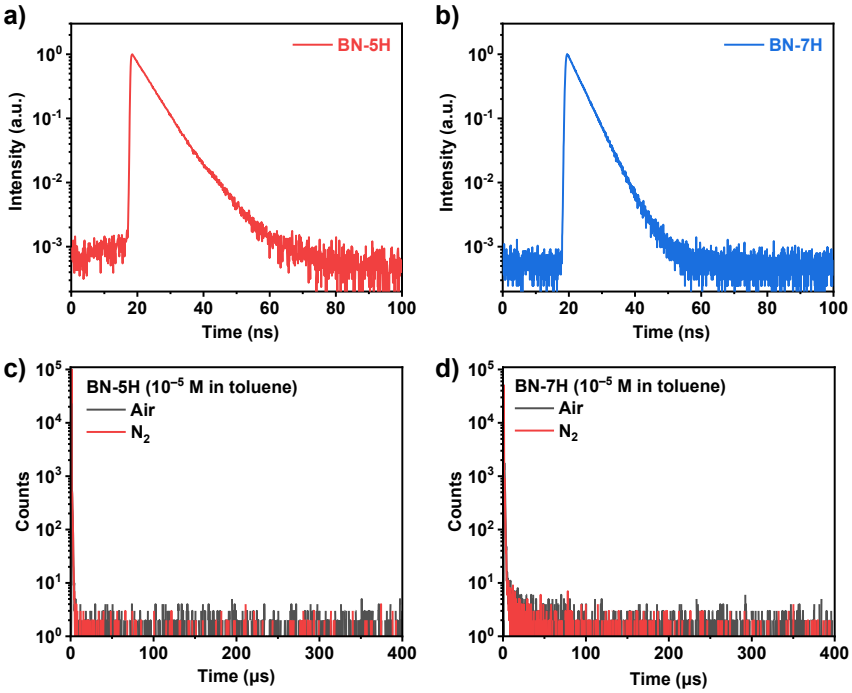


**Figure S5.** Transient photoluminescence decay curves of BN-5H and BN-7H in the toluene solutions ($1\times10^{-5}$ M) at 298 K.

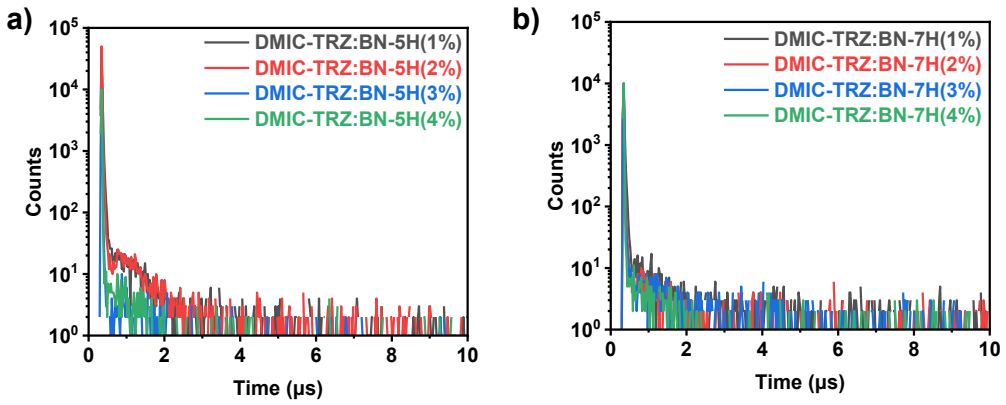


**Figure S6.** Transient photoluminescence decay curves of (a) BN-5H and (b) BN-7H doped in DMIC-TRZ films with different dopant concentrations. DMIC-TRZ: 1,3-dihydro-1,1-dimethyl-3-(3-(4,6-diphenyl-1,3,5-triazin-2-yl)phenyl)indeno[2,1-*b*]carbazole.

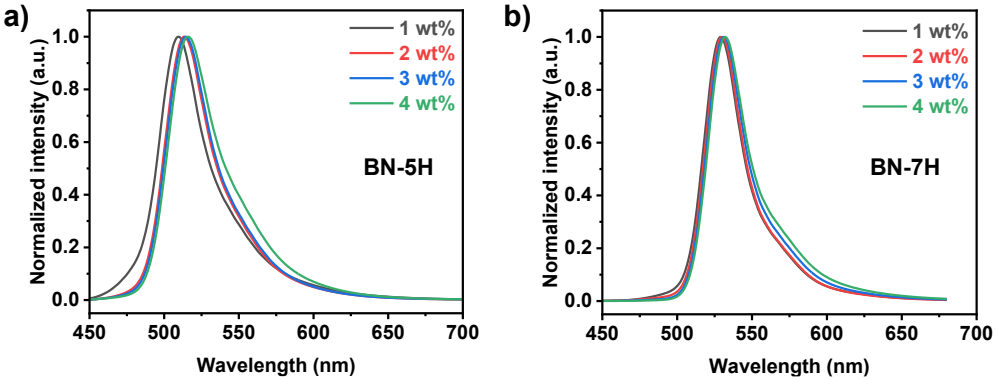


**Figure S7.** Normalized photoluminescence (PL) spectra of (a) BN-5H and (b) BN-7H in DMIC-TRZ: 30 wt% 3CTF films with different dopant concentrations. 3CTF: 2,4,6-tris(2-(3,6-di-*tert*-butyl-9*H*-carbazol-9-yl)-5-(trifluoromethyl)phenyl)-1,3,5-triazine.

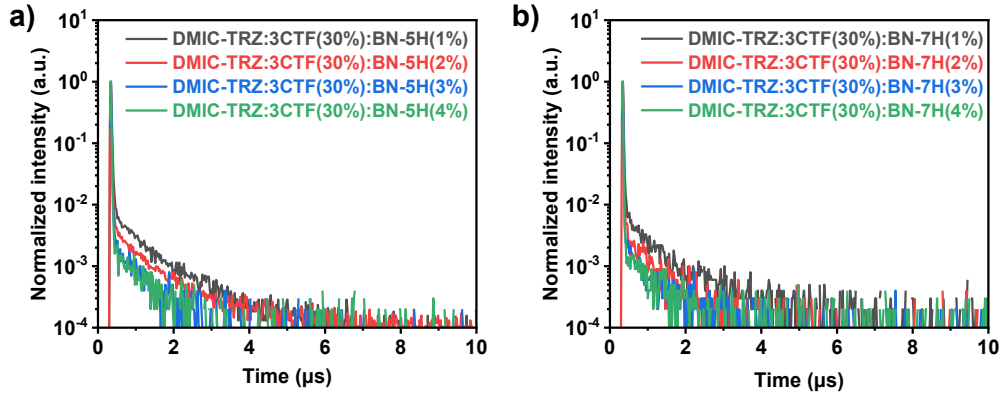


**Figure S8.** Transient photoluminescence decay curves of (a) BN-5H and (b) BN-7H in DMIC-TRZ: 30 wt% 3CTF films with different dopant concentrations.

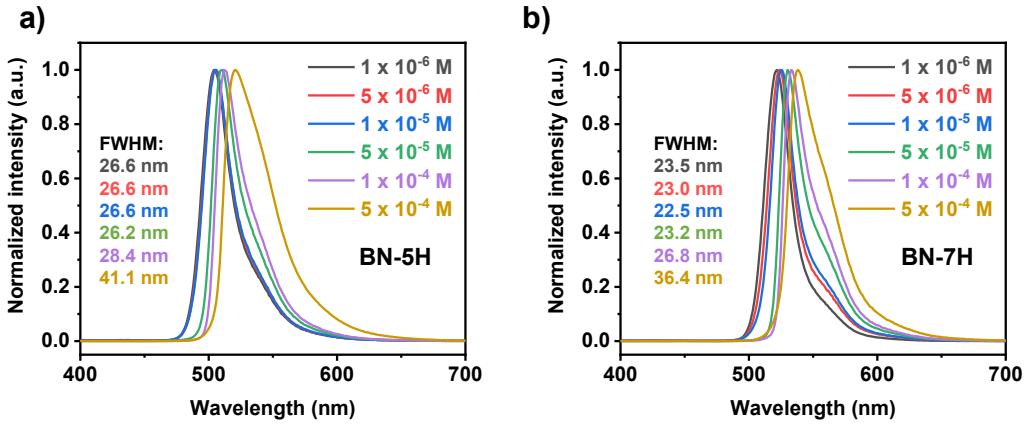


**Figure S9.** Normalized photoluminescence spectra of BN-5H and BN-7H in toluene solutions at different concentrations. At the concentration below $5 \times 10^{-5}$ M, the emission spectra of both compounds exhibit a gradual redshift of emission maximum with minor fluctuations of the FWHM. Upon further increasing the concentration, the emission spectra of BN-5H are significantly broadened with FWHM increasing from 26.2 nm to 41.1 nm. In contrast, BN-7H displays smaller changes in FWHMs over the same high-concentration range. These results are consistent with the trends in solid-state films and thus indicate the positive effect of twisted structure on suppressing spectral broadening.

**Table S2.** PLQYs of the doped films for BN-5H and BN-7H with different dopant concentrations.

| Doped film | PLQY (%) | Doped film | PLQY (%) |
|---|---|---|---|
| DMIC-TRZ:1 wt% BN-5H | 93 | DMIC-TRZ:1 wt% BN-7H | 94 |
| DMIC-TRZ:2 wt% BN-5H | 91 | DMIC-TRZ:2 wt% BN-7H | 93 |
| DMIC-TRZ:3 wt% BN-5H | 89 | DMIC-TRZ:3 wt% BN-7H | 91 |
| DMIC-TRZ:4 wt% BN-5H | 85 | DMIC-TRZ:4 wt% BN-7H | 90 |
| DMIC-TRZ:30 wt% 3CTF:1 wt% BN-5H | 95 | DMIC-TRZ:30 wt% 3CTF:1 wt% BN-7H | 96 |
| DMIC-TRZ:30 wt% 3CTF:2 wt% BN-5H | 93 | DMIC-TRZ:30 wt% 3CTF:2 wt% BN-7H | 95 |
| DMIC-TRZ:30 wt% 3CTF:3 wt% BN-5H | 90 | DMIC-TRZ:30 wt% 3CTF:3 wt% BN-7H | 93 |
| DMIC-TRZ:30 wt% 3CTF:4 wt% BN-5H | 86 | DMIC-TRZ:30 wt% 3CTF:4 wt% BN-7H | 92 |

## 5. Theoretical Calculations

Theoretical calculations were performed using the Gaussian 09 software package.[3] All calculations were carried out using the density functional theory (DFT) method. The geometries were optimized at the B3LYP/6-31G(d,p) level, and the energies were calculated at the same level of theory. Time-dependent DFT (TD-DFT) calculations were performed at the B3LYP/6-311G(d,p) level. The electron excitation analysis of major molecular orbital transitions in all excited states were carried out by Multiwfn.[4] The hole-electron analysis were completed with Multiwfn program.[5] The root-mean-square deviation (RMSD) values were calculated by VMD 1.9.3.[6] The Huang-Rhys (HR) factors and reorganization energies ($\lambda$) for $S_1 \rightarrow S_0$ transition were conducted with the DUSHIN module in the Molecular Materials Property Prediction Package (MOMAP 2021A) software.[7-12] The molecular vibration vector diagrams and reduced density gradient (RDG) isosurfaces were rendered with VMD 1.9.3.

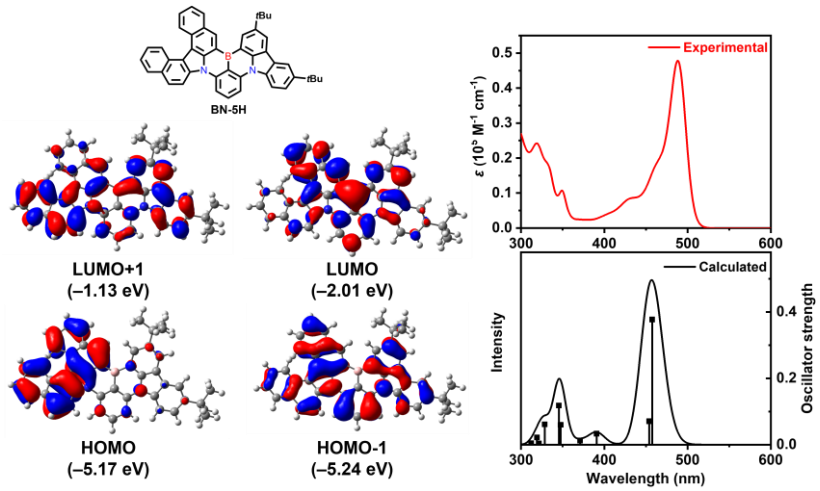


**Figure S10.** Theoretical absorption spectrum of BN-5H simulated at the B3LYP/6-311G(d,p) level (bottom) and the corresponding experimental absorption spectrum measured in toluene (top).

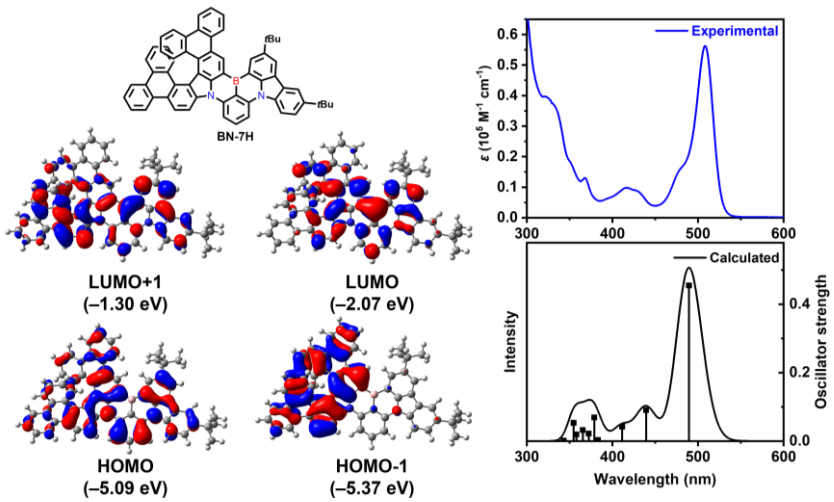


**Figure S11.** Theoretical absorption spectrum of BN-7H simulated at the B3LYP/6-311G(d,p) (bottom) and the corresponding experimental absorption spectrum measured in toluene (top).

**Table S3.** Summary of the TD-DFT calculation results of BN-5H at the optimized $S_0$ geometry.

| Excited States | Energy (eV) | Wavelength (nm) | Oscillator Strength | Major Contributions |
|---|---|---|---|---|
| $S_1$ | 2.7103 | 457.46 | 0.3773 | HOMO-1→LUMO (97%) |
| $S_2$ | 2.7318 | 453.86 | 0.0706 | HOMO→LUMO (97%) |
| $S_3$ | 3.1730 | 390.75 | 0.0333 | HOMO-2→LUMO (94%) |
| $S_4$ | 3.3422 | 370.97 | 0.0123 | HOMO-3→LUMO (97%) |
| $S_5$ | 3.5665 | 347.64 | 0.0598 | HOMO-1→LUMO+1 (56%)<br>HOMO→LUMO+1 (34%) |
| $S_6$ | 3.5899 | 345.37 | 0.1179 | HOMO→LUMO+1 (58%)<br>HOMO-1→LUMO+1 (32%) |
| $S_7$ | 3.7744 | 328.49 | 0.0614 | HOMO-4→LUMO (89%) |
| $S_8$ | 3.8564 | 321.50 | 0.0038 | HOMO-1→LUMO+2 (46%)<br>HOMO-2→LUMO+1 (23%)<br>HOMO→LUMO+3 (16%) |
| $S_9$ | 3.8860 | 319.05 | 0.0220 | HOMO-5→LUMO (35%)<br>HOMO→LUMO+2 (35%) |
| $S_{10}$ | 3.9709 | 312.23 | 0.0042 | HOMO→LUMO+2 (42%)<br>HOMO-5→LUMO (31%)<br>HOMO-1→LUMO+2 (7%) |

**Table S4.** Summary of the TD-DFT calculation results of BN-7H at the optimized $S_0$ geometry.

| Excited States | Energy (eV) | Wavelength (nm) | Oscillator Strength | Major Contributions |
|---|---|---|---|---|
| $S_1$ | 2.5332 | 489.44 | 0.4551 | HOMO→LUMO (97%) |
| $S_2$ | 2.8221 | 439.33 | 0.0904 | HOMO-1→LUMO (97%) |
| $S_3$ | 3.0147 | 411.27 | 0.0420 | HOMO-2→LUMO (92%) |
| $S_4$ | 3.2364 | 383.09 | 0.0031 | HOMO-3→LUMO (89%) |
| $S_5$ | 3.2740 | 378.69 | 0.0688 | HOMO→LUMO+1 (89%) |
| $S_6$ | 3.3309 | 372.22 | 0.0221 | HOMO-4→LUMO (90%) |
| $S_7$ | 3.3932 | 365.39 | 0.0322 | HOMO-5→LUMO (69%)<br>HOMO-6→LUMO (22%) |
| $S_8$ | 3.4649 | 357.83 | 0.0192 | HOMO-6→LUMO (55%)<br>HOMO-5→LUMO (21%)<br>HOMO-1→LUMO+1 (15%) |
| $S_9$ | 3.4959 | 354.66 | 0.0532 | HOMO-1→LUMO+1 (67%)<br>HOMO-6→LUMO (17%)<br>HOMO→LUMO+2 (6%) |
| $S_{10}$ | 3.6149 | 342.98 | 0.0013 | HOMO-7→LUMO (69%)<br>HOMO-2→LUMO+1 (10%)<br>HOMO-1→LUMO+2 (6%) |

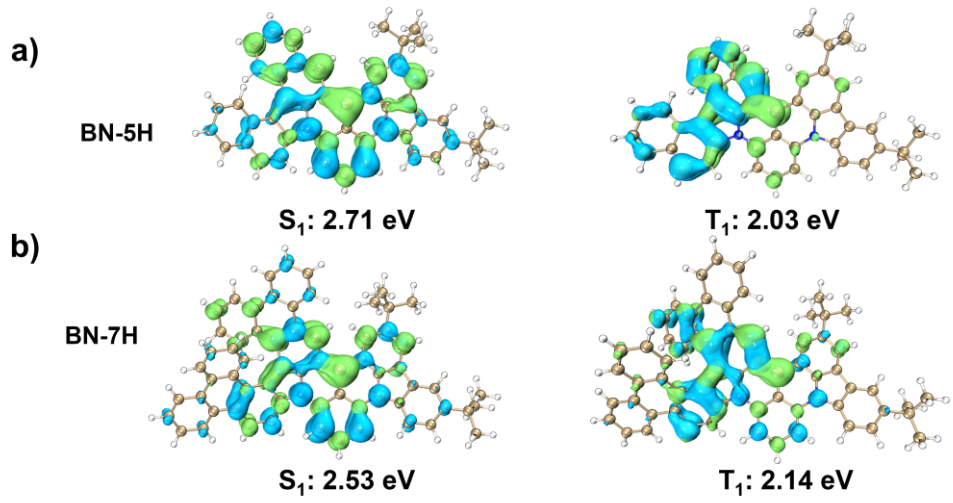


c) Contribution of each fragment to hole and electron

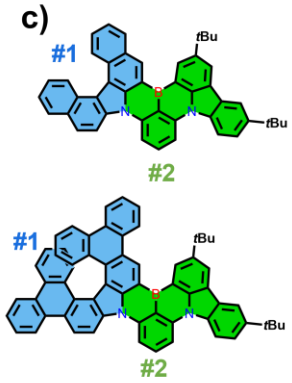


| | | $S_1$ | | $T_1$ | |
|---|---|---|---|---|---|
| | | #1 | #2 | #1 | #2 |
| BN-5H | Hole | 44.52% | 68.27% | 95.86% | 15.95% |
| | Electron | 41.82% | 60.30% | 72.30% | 33.63% |
| | Overlap | 43.15% | 64.16% | 83.25% | 23.16% |
| BN-7H | Hole | 55.65% | 58.37% | 79.88% | 32.30% |
| | Electron | 55.87% | 46.98% | 70.94% | 33.87% |
| | Overlap | 55.76% | 52.37% | 75.28% | 33.08% |

**Figure S12.** Hole (blue) and electron (green) distributions of (a) BN-5H and (b) BN-7H at $S_0$ and $T_1$ states (Isovalue: 0.001). (c) The contribution of each fragment to the hole and electron. The $S_1$ state of both two molecules exhibits well-separated hole and electron distributions, which is consistent with their frontier molecular orbital (FMO) distribution. However, an obvious difference emerges in their $T_1$ states. The hole and electron are mainly localized at the 5H fragment in BN-5H. In contrast, for BN-7H with the extended [7]helicene skeleton, the $T_1$ state shows a more dispersed distribution, with significant density on the benzene rings connected to the B/N unit. The different orbital distribution characteristics endow BN-5H with a lower $T_1$ energy.

To quantitatively analyze the contribution of each fragment to the hole and electron, the molecular structures of these two compounds are divided into two fragments. The hole contribution from fragment #1 at the $S_1$ state shows an evident increase from 44.52% for BN-5H to 55.65% for BN-7H, and similar results are obtained for the electron distribution. The higher overlap of hole and electron in BN-7H at the $S_1$ state enables a larger oscillator strength (*f*),[13] which has been proved in the TD-DFT calculation results. On the other hand, the contribution of hole and electron from the fragment #2 of BN-5H and BN-7H cannot be ignored. The reduced spatial overlap between hole and electron at $S_1$ state in BN-7H is observed. This will lead to a smaller exchange integral and achieve smaller $\Delta E_{ST}$.[14] According to the above results, the reduction of $\Delta E_{ST}$ of BN-7H is attributed to the different orbital distribution characteristics.

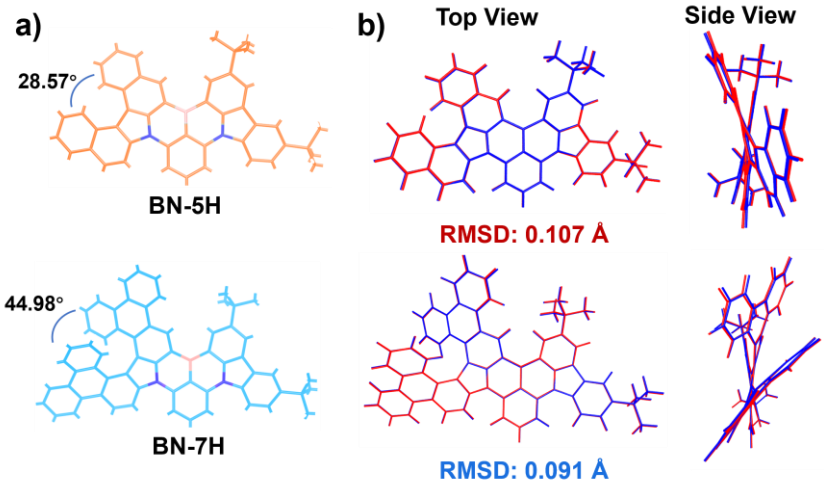


**Figure S13.** (a) Optimized ground-state geometries of BN-5H and BN-7H. (b) Comparison of the optimized $S_0$ (blue) and $S_1$ (red) geometries of BN-5H and BN-7H.

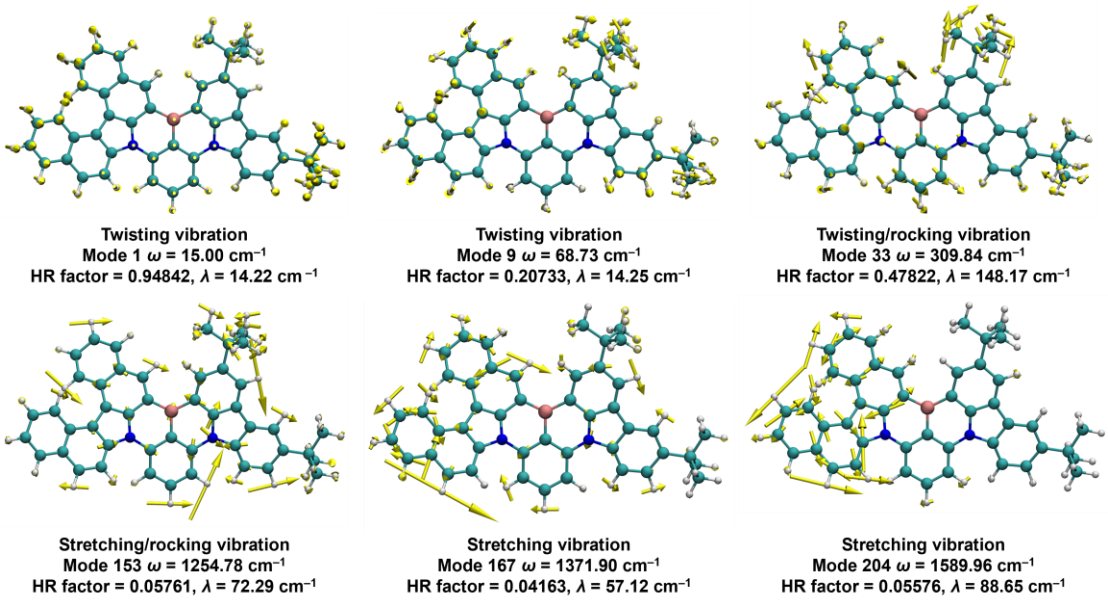


**Figure S14.** The major vibrational modes of BN-5H for the $S_1 \rightarrow S_0$ transition. $\omega$, HR factor and $\lambda$ represent vibration frequency, Huang-Rhys factor and reorganization energy of selected vibrational mode, respectively.

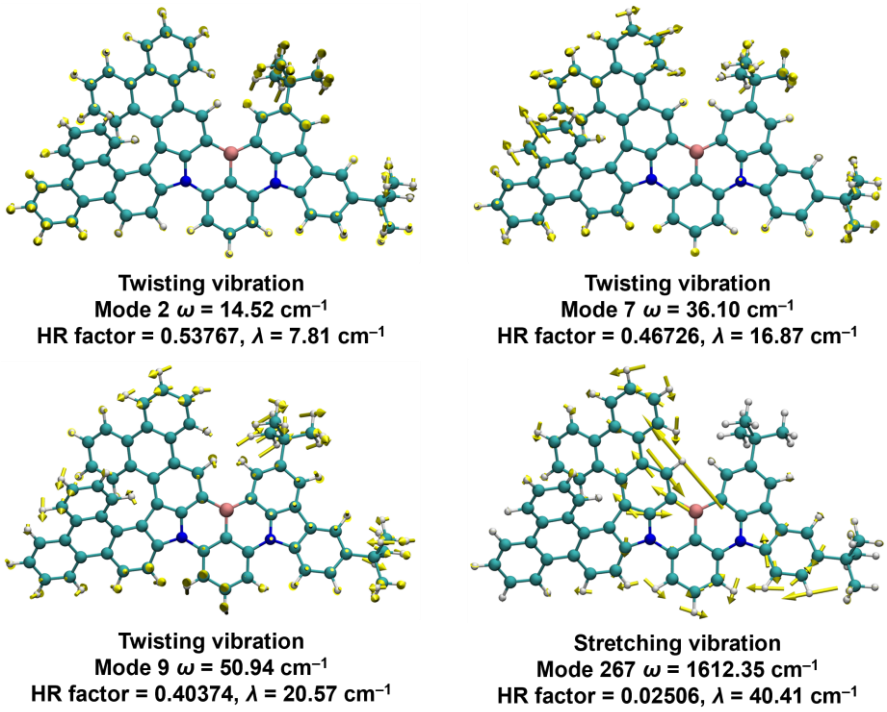


**Figure S15.** The major vibrational modes of BN-7H for $S_1 \rightarrow S_0$ transition.

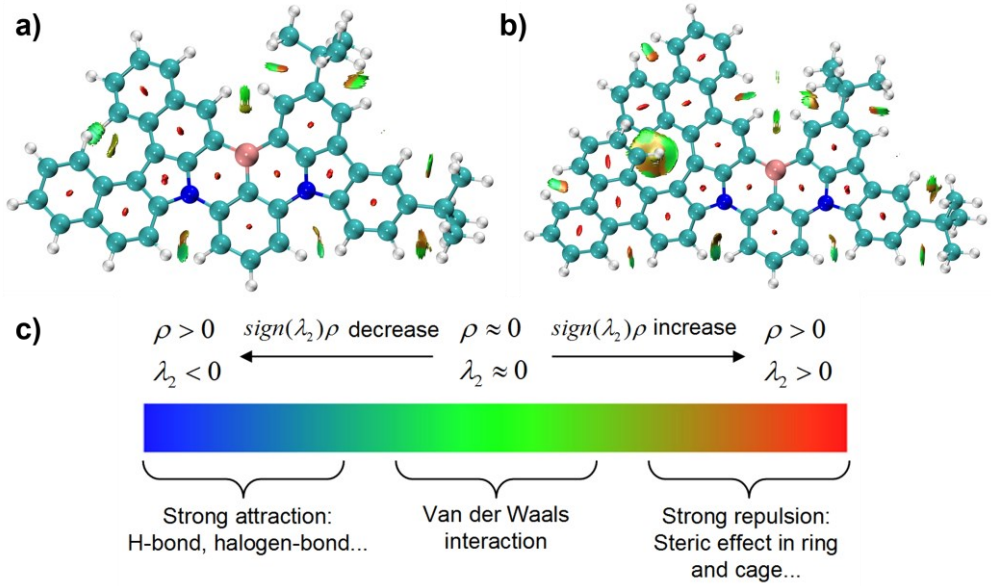


**Figure S16.** Calculated reduced density gradient (RDG) isosurfaces based on the optimized $S_0$ geometries of (a) BN-5H and (b) BN-7H. (c) Standard coloring method and chemical explanation of sign($\lambda_2$)$\rho$ on RDG isosurface.

**Cartesian coordinates obtained in gas-phase DFT calculations**

**BN-5H ($S_0$)**

*E*(B3LYP/6-31G(d,p)) = –1909.735625 Hartree

| Tag | Symbol | X | Y | Z |
|---|---|---|---|---|
| 1 | C | –4.49692172 | –0.30264584 | –0.07995647 |

| | | | | |
|---|---|---|---|---|
| 2 | C | –5.89234782 | –0.36024059 | –0.05208176 |
| 3 | C | –6.54851639 | –1.54754987 | 0.28338200 |
| 4 | C | –5.74694467 | –2.65818333 | 0.61636392 |
| 5 | C | –4.35382595 | –2.63073731 | 0.59216594 |
| 6 | C | –3.71427523 | –1.44881102 | 0.20715177 |
| 7 | C | –1.32770773 | 2.41592624 | –0.53100112 |
| 8 | C | –2.59461684 | 2.98022896 | –0.73305693 |
| 9 | C | –3.72635593 | 2.14656214 | –0.60365490 |
| 10 | C | –3.57866597 | 0.79637587 | –0.31138323 |
| 11 | C | –1.12075805 | 1.05170457 | –0.22012233 |
| 12 | C | –2.27989102 | 0.27173092 | –0.15541938 |
| 13 | N | –2.34087976 | –1.09784639 | 0.10469611 |
| 14 | C | 0.08325163 | –1.23531420 | 0.09773503 |
| 15 | C | –1.18439942 | –1.89381454 | 0.12796571 |
| 16 | C | –1.26128152 | –3.29437124 | 0.16089197 |
| 17 | C | –0.09343443 | –4.03436266 | 0.28378756 |
| 18 | C | 1.16182157 | –3.43210952 | 0.30348334 |
| 19 | C | 1.25693696 | –2.04678382 | 0.13513268 |
| 20 | N | 2.51165941 | –1.40586119 | 0.03515168 |
| 21 | C | 3.79299467 | –1.94070570 | –0.19114542 |
| 22 | C | 4.75744721 | –0.91850828 | –0.02441914 |
| 23 | C | 4.03098403 | 0.27841561 | 0.37602936 |
| 24 | C | 2.66836246 | –0.04638808 | 0.28520743 |
| 25 | C | 4.14477249 | –3.24056911 | –0.62128447 |
| 26 | C | 5.46925314 | –3.52852994 | –0.83582836 |
| 27 | C | 6.47881967 | –2.53198049 | –0.73710723 |
| 28 | C | 6.12108024 | –1.18280607 | –0.39681783 |
| 29 | C | 4.35852410 | 1.57973705 | 0.88636824 |
| 30 | C | 3.28700099 | 2.53867266 | 1.00551573 |
| 31 | C | 1.94930238 | 2.17113212 | 0.70133780 |
| 32 | C | 1.59242495 | 0.87265671 | 0.36900164 |
| 33 | C | 5.63193805 | 1.96098789 | 1.38788568 |
| 34 | C | 5.86596097 | 3.23020927 | 1.87467229 |
| 35 | C | 4.83789870 | 4.19863616 | 1.89512859 |
| 36 | C | 3.57434331 | 3.84705846 | 1.48149007 |
| 37 | C | 7.82500886 | –2.83939474 | –1.06466171 |
| 38 | C | 8.78663685 | –1.85672264 | –1.12857299 |
| 39 | C | 8.41821830 | –0.51410818 | –0.89795082 |
| 40 | C | 7.12376158 | –0.18820850 | –0.54908464 |
| 41 | B | 0.18948868 | 0.30190127 | 0.07045405 |
| 42 | C | –2.79698039 | 4.46843254 | –1.08204559 |
| 43 | C | –1.46544236 | 5.23636832 | –1.18146666 |
| 44 | C | –3.65809436 | 5.14388504 | 0.01177675 |
| 45 | C | –3.51881720 | 4.58453694 | –2.44578705 |

| | | | | |
|---|---|---|---|---|
| 46 | C | –8.08268939 | –1.67356410 | 0.32186582 |
| 47 | C | –8.78517452 | –0.36071279 | –0.07228050 |
| 48 | C | –8.53684312 | –2.05185836 | 1.75170110 |
| 49 | C | –8.53327572 | –2.77529347 | –0.66657268 |
| 50 | H | –6.45442650 | 0.53716492 | –0.28340406 |
| 51 | H | –6.22259987 | –3.58609117 | 0.91825003 |
| 52 | H | –3.81242460 | –3.50810661 | 0.91392874 |
| 53 | H | –0.45157138 | 3.04332718 | –0.63292635 |
| 54 | H | –4.72263039 | 2.55828900 | –0.73609530 |
| 55 | H | –2.20485339 | –3.80754495 | 0.07366811 |
| 56 | H | –0.16009349 | –5.11534414 | 0.36589924 |
| 57 | H | 2.03722541 | –4.03828525 | 0.47557243 |
| 58 | H | 3.39666982 | –3.99194839 | –0.82433210 |
| 59 | H | 5.75642689 | –4.52700364 | –1.15316960 |
| 60 | H | 1.18259111 | 2.93418459 | 0.79613124 |
| 61 | H | 6.42329696 | 1.22540221 | 1.43638869 |
| 62 | H | 6.84948568 | 3.48063284 | 2.26189768 |
| 63 | H | 5.03856057 | 5.19930360 | 2.26545197 |
| 64 | H | 2.75852214 | 4.56334328 | 1.53680709 |
| 65 | H | 8.07715811 | –3.87196106 | –1.29253486 |
| 66 | H | 9.81137197 | –2.10487975 | –1.38802275 |
| 67 | H | 9.15596970 | 0.27503485 | –1.01123318 |
| 68 | H | 6.85997424 | 0.85313377 | –0.43156249 |
| 69 | H | –0.81475218 | 4.82733264 | –1.96098809 |
| 70 | H | –1.66301566 | 6.28333048 | –1.43293852 |
| 71 | H | –0.91569877 | 5.22393197 | –0.23462183 |
| 72 | H | –4.64288280 | 4.67631881 | 0.10428064 |
| 73 | H | –3.81503244 | 6.20226703 | –0.22503439 |
| 74 | H | –3.16757892 | 5.08317013 | 0.98871342 |
| 75 | H | –3.67688278 | 5.63716849 | –2.70640211 |
| 76 | H | –2.92649075 | 4.12245280 | –3.24215137 |
| 77 | H | –4.49760660 | 4.09583158 | –2.43248763 |
| 78 | H | –8.52266069 | –0.04757193 | –1.08812090 |
| 79 | H | –9.87053372 | –0.49922421 | –0.04004662 |
| 80 | H | –8.53766938 | 0.45622026 | 0.61349498 |
| 81 | H | –8.10692820 | –3.00333746 | 2.07804383 |
| 82 | H | –9.62760824 | –2.14896529 | 1.79254794 |
| 83 | H | –8.23641819 | –1.28531047 | 2.47331882 |
| 84 | H | –8.23311723 | –2.52918633 | –1.69028589 |
| 85 | H | –8.09983976 | –3.74827675 | –0.41719953 |
| 86 | H | –9.62373752 | –2.88225488 | –0.64807723 |

**BN-7H ($S_0$)**

*E*(B3LYP/6-31G(d,p)) = –2524.309571 Hartree

| Tag | Symbol | X | Y | Z |
|---|---|---|---|---|
| 1 | C | 5.36612629 | 0.45514961 | –0.32754366 |
| 2 | C | 5.53281019 | 1.80103239 | –0.64847952 |
| 3 | C | 4.41152628 | 2.62411338 | –0.85857932 |
| 4 | C | 3.13274750 | 2.05915314 | –0.70605054 |
| 5 | C | 2.90730596 | 0.70918438 | –0.36779150 |
| 6 | C | 4.06465510 | –0.06708344 | –0.22393480 |
| 7 | C | 7.48838450 | –2.98088829 | 0.78229541 |
| 8 | C | 8.30206305 | –1.87894551 | 0.46866139 |
| 9 | C | 7.66086358 | –0.69621783 | 0.07530112 |
| 10 | C | 6.27288309 | –0.63623967 | –0.02550942 |
| 11 | C | 6.09411331 | –2.95103521 | 0.68642903 |
| 12 | C | 5.47591919 | –1.78042839 | 0.24717665 |
| 13 | N | 4.11057404 | –1.43122308 | 0.06919702 |
| 14 | C | 1.68772130 | –1.56994188 | –0.03787430 |
| 15 | C | 2.95407742 | –2.22717925 | 0.05353212 |
| 16 | C | 3.03069587 | –3.62620392 | 0.10454487 |
| 17 | C | 1.85901247 | –4.36764237 | 0.18485569 |
| 18 | C | 0.60404274 | –3.76782717 | 0.15399085 |
| 19 | C | 0.51422946 | –2.38177185 | –0.02210561 |
| 20 | B | 1.58209440 | –0.03577085 | –0.12442450 |
| 21 | N | –0.73784911 | –1.74347058 | –0.15120852 |
| 22 | C | –2.02236441 | –2.30378371 | –0.27999834 |
| 23 | C | –2.99825192 | –1.30233304 | –0.04144077 |
| 24 | C | –2.27061566 | –0.02868686 | 0.00717768 |
| 25 | C | –0.89875404 | –0.37173944 | –0.00906119 |
| 26 | C | –2.39072845 | –3.58878325 | –0.70299681 |
| 27 | C | –3.73490191 | –3.88205926 | –0.80816742 |
| 28 | C | –4.73984770 | –2.98314859 | –0.38272350 |
| 29 | C | –4.36125181 | –1.71220069 | 0.12904749 |
| 30 | C | –2.59342111 | 1.36236458 | –0.04110204 |
| 31 | C | –1.55578383 | 2.28884357 | 0.29005941 |
| 32 | C | –0.21362494 | 1.86525307 | 0.29197227 |
| 33 | C | 0.16640571 | 0.54262861 | 0.05448054 |
| 34 | C | –3.85860524 | 1.91372871 | –0.53086347 |
| 35 | C | –4.17020590 | 3.28657694 | –0.32526070 |
| 36 | C | –3.22704117 | 4.14724654 | 0.38980877 |
| 37 | C | –1.91059339 | 3.67398620 | 0.62533191 |
| 38 | C | –6.16149731 | –3.32332782 | –0.50429645 |
| 39 | C | –7.14649440 | –2.46091475 | 0.04584891 |
| 40 | C | –6.72135896 | –1.32588974 | 0.86435372 |
| 41 | C | –5.34842721 | –0.95703802 | 0.90305176 |
| 42 | C | –3.57122691 | 5.44722445 | 0.81609703 |
| 43 | C | –2.64870882 | 6.27629607 | 1.43137067 |

| | | | | |
|---|---|---|---|---|
| 44 | C | –1.34308863 | 5.81735700 | 1.64873220 |
| 45 | C | –0.98911213 | 4.53655333 | 1.25852386 |
| 46 | C | –6.59287234 | –4.46218650 | –1.22114791 |
| 47 | C | –7.93571142 | –4.73843548 | –1.41029243 |
| 48 | C | –8.90543153 | –3.86967738 | –0.89215913 |
| 49 | C | –8.50935908 | –2.75169228 | –0.17962832 |
| 50 | C | –7.63548985 | –0.61916336 | 1.67487072 |
| 51 | C | –7.22455281 | 0.39862143 | 2.51768277 |
| 52 | C | –5.86467116 | 0.72521261 | 2.59711273 |
| 53 | C | –4.95009070 | 0.05204866 | 1.80744902 |
| 54 | C | –5.87873886 | 1.67548161 | –1.88301177 |
| 55 | C | –6.21393507 | 3.01139787 | –1.63066656 |
| 56 | C | –5.36228150 | 3.80053295 | –0.87605543 |
| 57 | C | –4.71938988 | 1.14556621 | –1.34463911 |
| 58 | C | 9.83904932 | –1.92317588 | 0.56359478 |
| 59 | C | 10.44851186 | –1.60195146 | –0.82170508 |
| 60 | C | 10.32443069 | –0.87346299 | 1.59132670 |
| 61 | C | 10.35999135 | –3.30333959 | 1.00679577 |
| 62 | C | 4.54364024 | 4.11142766 | –1.24558393 |
| 63 | C | 3.87590372 | 4.34623362 | –2.62143251 |
| 64 | C | 6.01327932 | 4.56290183 | –1.34486116 |
| 65 | C | 3.84542721 | 4.99118906 | –0.18141019 |
| 66 | H | 6.53508185 | 2.20376764 | –0.73892629 |
| 67 | H | 2.26587216 | 2.68922460 | –0.87431984 |
| 68 | H | 7.94086587 | –3.90358812 | 1.12505009 |
| 69 | H | 8.24118502 | 0.19525816 | –0.14370594 |
| 70 | H | 5.53684739 | –3.82235129 | 0.99771143 |
| 71 | H | 3.97817382 | –4.13802784 | 0.06107200 |
| 72 | H | 1.92401677 | –5.44792381 | 0.27700243 |
| 73 | H | –0.27595497 | –4.37506018 | 0.29547799 |
| 74 | H | –1.65800526 | –4.31651716 | –1.01954558 |
| 75 | H | –4.00919448 | –4.85777964 | –1.18816460 |
| 76 | H | 0.56524525 | 2.60044122 | 0.44759602 |
| 77 | H | –4.58505542 | 5.80556783 | 0.67902130 |
| 78 | H | –2.94235172 | 7.27055689 | 1.75438847 |
| 79 | H | –0.61405343 | 6.45207224 | 2.14365354 |
| 80 | H | 0.00960846 | 4.18348388 | 1.48757772 |
| 81 | H | –5.86471767 | –5.12887788 | –1.66706691 |
| 82 | H | –8.23217286 | –5.61713839 | –1.97534788 |
| 83 | H | –9.96123587 | –4.06554377 | –1.05347129 |
| 84 | H | –9.27036243 | –2.07852676 | 0.19756037 |
| 85 | H | –8.68190563 | –0.90059158 | 1.67341917 |
| 86 | H | –7.95146931 | 0.91729125 | 3.13571985 |
| 87 | H | –5.52254785 | 1.49212049 | 3.28528874 |

| | | | | |
|---|---|---|---|---|
| 88 | H | –3.89897612 | 0.28591438 | 1.90644600 |
| 89 | H | –6.51431645 | 1.05760250 | –2.50982166 |
| 90 | H | –7.11965268 | 3.43938919 | –2.05012131 |
| 91 | H | –5.60377439 | 4.84890290 | –0.74539783 |
| 92 | H | –4.44928325 | 0.12576523 | –1.58084235 |
| 93 | H | 10.12939967 | –2.33531441 | –1.56937397 |
| 94 | H | 10.14944559 | –0.61180919 | –1.17807135 |
| 95 | H | 11.54308203 | –1.62112220 | –0.77166941 |
| 96 | H | 9.91277625 | –1.07894805 | 2.58476386 |
| 97 | H | 11.41765734 | –0.88877225 | 1.66599319 |
| 98 | H | 10.02527674 | 0.14057350 | 1.31021384 |
| 99 | H | 10.06893154 | –4.09302622 | 0.30644315 |
| 100 | H | 11.45372198 | –3.28755265 | 1.04975172 |
| 101 | H | 9.99608833 | –3.57679464 | 2.00258564 |
| 102 | H | 3.95520162 | 5.40054519 | –2.90990689 |
| 103 | H | 4.35869386 | 3.74410994 | –3.39802834 |
| 104 | H | 2.81412132 | 4.08394916 | –2.60888803 |
| 105 | H | 6.05523201 | 5.62146653 | –1.62035615 |
| 106 | H | 6.54077256 | 4.45007427 | –0.39180532 |
| 107 | H | 6.56175841 | 4.00284689 | –2.10940337 |
| 108 | H | 3.93595429 | 6.05136838 | –0.44353097 |
| 109 | H | 2.77896589 | 4.76213035 | –0.09862675 |
| 110 | H | 4.29718779 | 4.84508959 | 0.80524074 |

## 6. Device Fabrication and Measurement

All compounds were purified by temperature-gradient sublimation under a high vacuum before use. Organic light-emitting diodes (OLEDs) were fabricated on ITO-coated glass substrates with multiple organic layers sandwiched between the transparent bottom ITO anode and the top metal cathode. The ITO glass substrates were first cleaned carefully. Then different layers of organic materials were deposited by thermal evaporation in a vacuum chamber with a base pressure of $10^{-6}$ torr. The deposition system permits the fabrication of the complete device in a single vacuum pump-down without breaking vacuum. The deposition rate of organic layers was kept at 0.1-0.2 nm $s^{-1}$. The doping layer was obtained by co-evaporation from separate sources with different evaporation rates. The current density, voltage, luminance, current efficiency (CE), power efficiency (PE), external quantum efficiency (EQE), electroluminescence (EL) spectra and other device characteristics were measured at the same time with a Keithley 2400 source meter and a Hamamatsu C9920-12 instrument, which is equipped with Hamamatsu PMA-12 Photonic multichannel analyzer C10027-02.

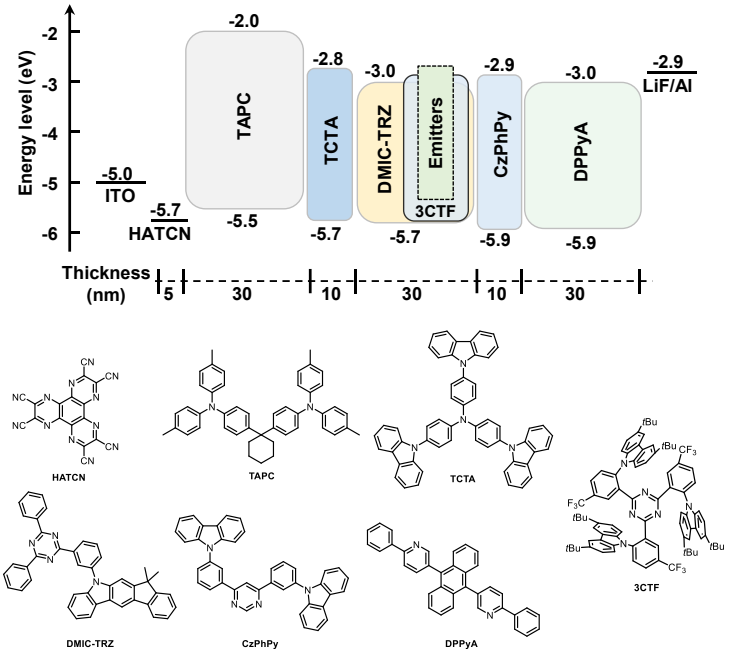


**Figure S17.** Device structure, the energy level diagram, and chemical structures of the materials utilized in the thermally activated delayed fluorescence (TADF)-sensitized OLED device. The sensitized OLEDs were fabricated with the following device structure: indium tin oxide (ITO)/dipyrazino[2,3-*f*:2',3'-*h*]quinoxaline-2,3,6,7,10,11-hexacarbonitrile (HATCN) (5 nm)/1,1-bis[(di-4-tolylamino)phenyl]cyclohexane (TAPC) (30 nm)/tri(4-carbazoly-9-ylphenyl)amine (TCTA) (10 nm)/emitting layer (EML, 30 nm)/4,6-bis(3-(9*H*-carbazol-9-yl)phenyl)pyrimidine (CzPhPy) (10 nm)/9,10-bis(6-phenylpyridin-3-yl)anthracene (DPPyA) (30 nm)/LiF (0.5 nm)/Al (150 nm). Among the materials used, HATCN and TAPC were employed as the hole injection and transporting materials while LiF and DPPyA as the electron injection and

transporting materials, respectively. Meanwhile, TCTA and CzPhPy were used as the electron- and hole-blocking layers. DMIC-TRZ was adopted as the host material. 3CTF was chosen as the TADF sensitizer because of its small molecular dipole moment, significant spectral overlap with these emitters, and high reverse intersystem crossing rate of $2.57\times10^{6}$ $s^{-1}$.[15]

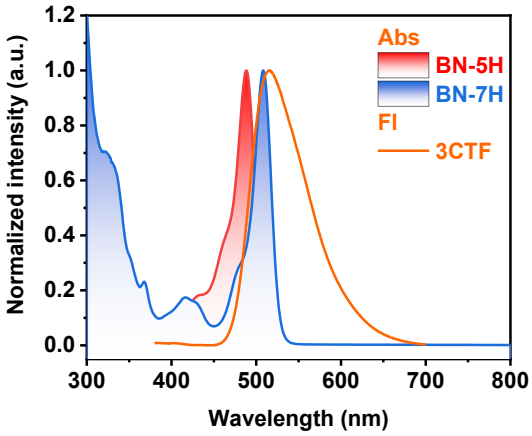


**Figure S18.** UV-vis absorption spectra of the MR emitters and the fluorescence spectrum of the sensitizer 3CTF in toluene solution. Significant absorption-emission spectral overlap between the emitter and the TADF sensitizer is observed, suggesting the possibility of efficient energy transfer from 3CTF to BN-5H and BN-7H.

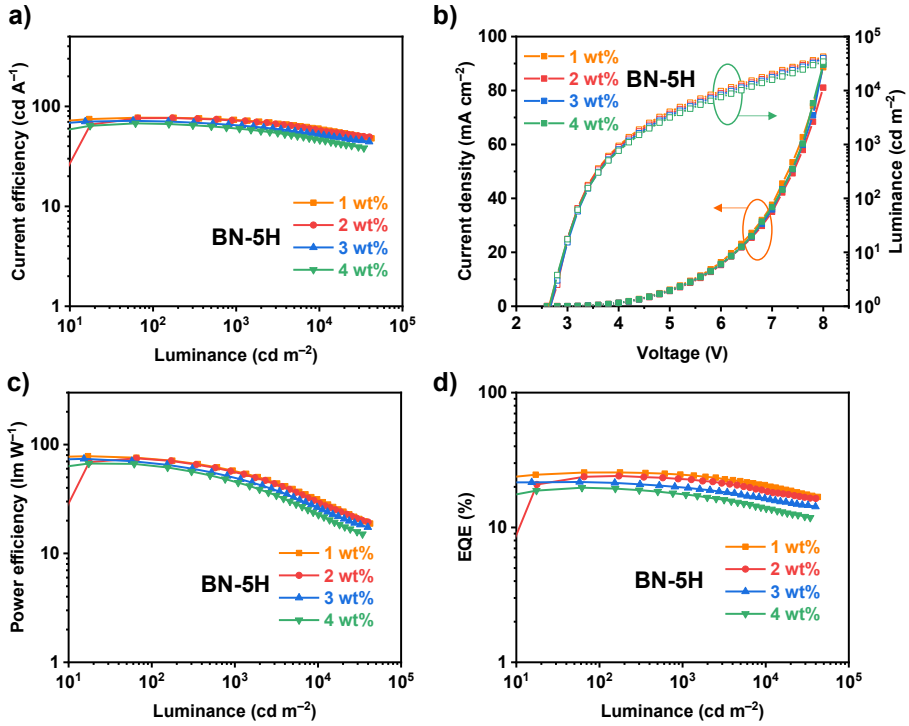


**Figure S19.** (a) Current efficiency versus luminance, (b) current density and luminance versus voltage, (c) power efficiency versus luminance, and (d) external quantum efficiency (EQE) versus luminance curves of the sensitized OLED devices based on BN-5H.

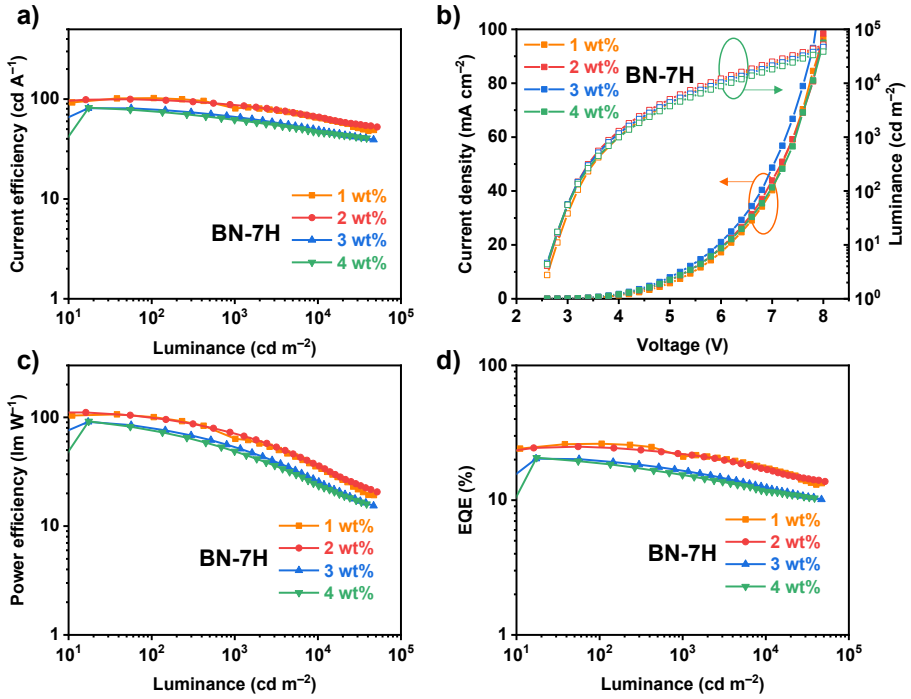


**Figure S20.** (a) Current efficiency versus luminance, (b) current density and luminance versus voltage, (c) power efficiency versus luminance, and (d) external quantum efficiency (EQE) versus luminance curves of the sensitized OLED devices based on BN-7H.

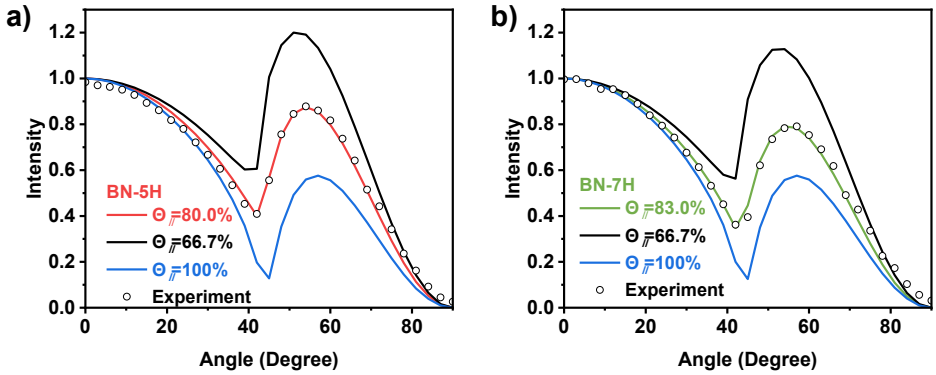


**Figure S21.** Angle-dependent PL spectra of the *p*-polarized light of the emitting layers ($\Theta_{//}$ = 66.7% denotes isotropic emitting dipole orientation, $\Theta_{//}$ = 100% denotes completely horizontal emitting dipole orientation).

**Table S5.** Summary of sensitized green OLEDs device data of the reported MR emitters with FWHM < 30 nm.

| Emitter | $\lambda_{EL}$[a] [nm] | $FWHM_{EL}$ [b] [nm] | CIE(x,y) | Reference |
|---|---|---|---|---|
| **BN-5H** | **507** | **34** | **(0.19,0.62)** | **This work** |
| **BN-7H** | **527** | **28** | **(0.24,0.69)** | |
| tCzphB-Fl | 535 | 26 | (0.26,0.72) | *Nat. Commun*. **2022**, *13*, 4876. |
| tCzphB-Ph | 527 | 24 | (0.21,0.75) | |
| BN-ICz-1 | 523 | 23 | (0.22,0.74) | *Angew. Chem. Int. Ed.* **2022**, *61*, e202202380. |
| BN-ICz-2 | 523 | 23 | (0.21,0.73) | |
| IDID2BN | 534 | 29 | (0.31,0.65) | *Angew. Chem. Int. Ed.* **2023**, *62,* e202313254. |
| BpIC-DPA | 536 | 29 | (0.30,0.67) | *Chem. Eng. J.* **2024**, *481*, 148781. |
| DBSe-BN | 518 | 25 | (0.22,0.71) | *Adv. Mater.* **2025**, DOI: 10.1002/adma.202513987. |
| ω-DABNA-PH | 522 | 29 | (0.21,0.69) | *Nat. Commun.* **2024**, *15,* 3174. |
| ω-DABNA-M | 517 | 23 | (0.17,0.70) | |
| TPABO-DICz | 522 | 22 | (0.24,0.74) | *Angew. Chem. Int. Ed.* **2024**, *63,* e202318742. |
| DBNO | 504 | 27 | (0.14,0.53) | *Angew. Chem. Int. Ed.* **2022**, *61*, e202200337. |
| *ββ*ICZ | 508 | 19 | (0.22,0.64) | *Adv. Mater.* **2023**, *35,* 2211316. |
| *ββ*CNICZ | 509 | 19 | (0.21,0.65) | |
| DBN-NaMe | 514 | 20 | (0.18,0.70) | *Adv. Mater.* **2025**, *37,* 2411610. |
| DBN-NaPh | 526 | 20 | (0.23,0.72) | |
| DBN-NaPh-d | 526 | 19 | (0.21,0.74) | |
| BN-ANAP | 524 | 29 | (0.26,0.67) | *Sci. China Mater.* **2024**, *67*, 1581. |
| ω'-DABNA | 518 | 26 | (0.21,0.72) | *Angew. Chem. Int. Ed.* **2025**, *64*, e202512162. |
| ω'-DABNA-D | 519 | 26 | (0.20,0.72) | |
| DBNDS-TPh | 523 | 20.3 | (0.20, 0.73) | *Adv. Mater.* **2025**, *37*, 2416224. |
| DBNDS-DFPh | 523 | 20.2 | (0.19,0.75) | |
| DBNDS-CNPh | 521.5 | 21.8 | (0.21,0.71) | |

[a] EL peak wavelength. [b] Full-width at half-maximum of the EL spectra.

## 7. Optical Resolution and Chiroptical Properties

Chiral high-performance liquid chromatography (HPLC) was implemented on a Daicel Chiralpak IE column. Circular dichroism (CD) spectra were collected on BioLogic MOS-450 circular dichroism spectrometer at 297 K. Circularly polarized luminescence (CPL) measurements were performed using JASCO CPL-300 at 297 K.

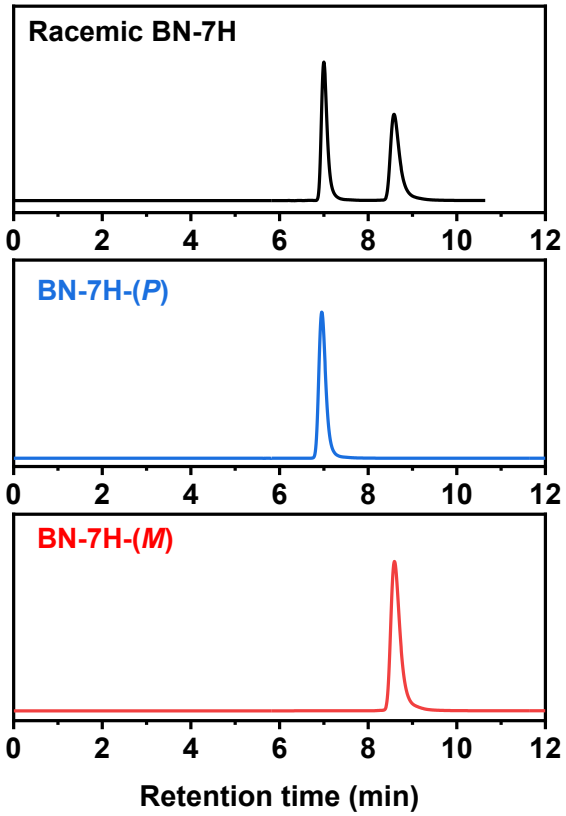


**Figure S22.** Chiral HPLC analysis of racemic BN-7H, BN-7H-(*P*), and BN-7H-(*M*) eluted by $CH_2Cl_2$ using Daicel Chiralpak IE column. Elution rate: 0.5 mL $min^{-1}$. The integration areas of the (*P*) and (*M*)- enantiomers are 50.0% and 49.7%, respectively.

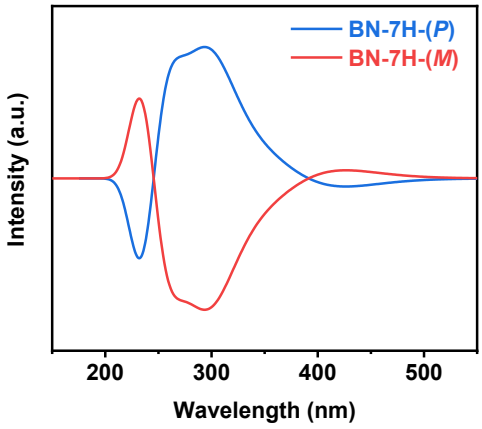


**Figure S23.** Simulated CD spectra of BN-7H (FWHM = 726 $cm^{-1}$). The simulated CD spectra were obtained by TD-DFT calculations at the M062X/6-311G(d) level.

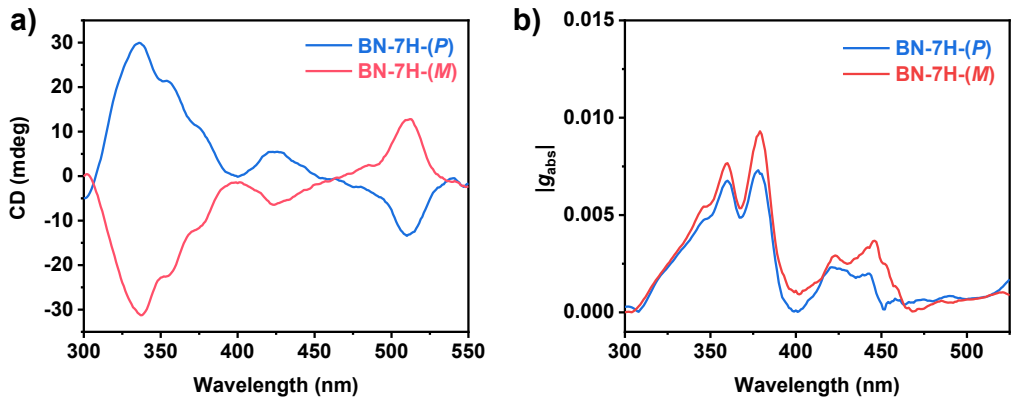


**Figure S24.** (a) CD spectra of BN-7H in toluene solution (c = $9.0\times10^{-6}$ M), and (b) the corresponding absolute absorption dissymmetry factors ($|g_{abs}|$).

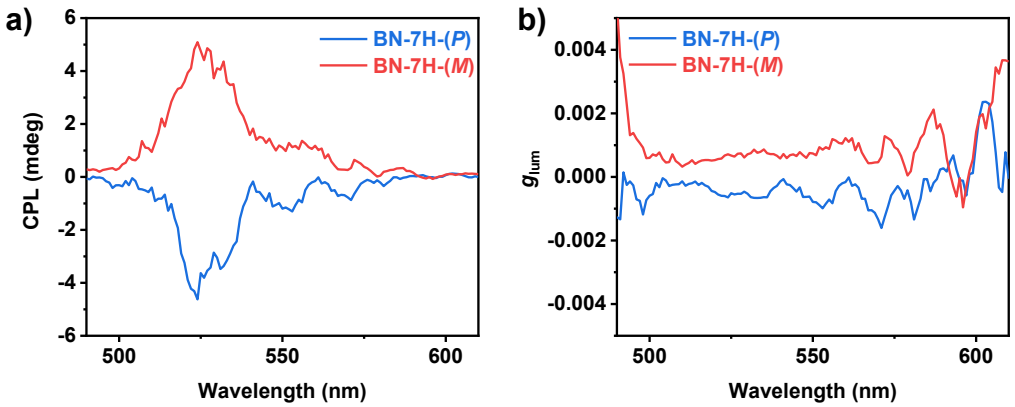


**Figure S25.** (a) CPL spectra of BN-7H in toluene solution (c = $9.0\times10^{-6}$ M), and (b) the corresponding luminescence dissymmetry factors ($g_{lum}$).

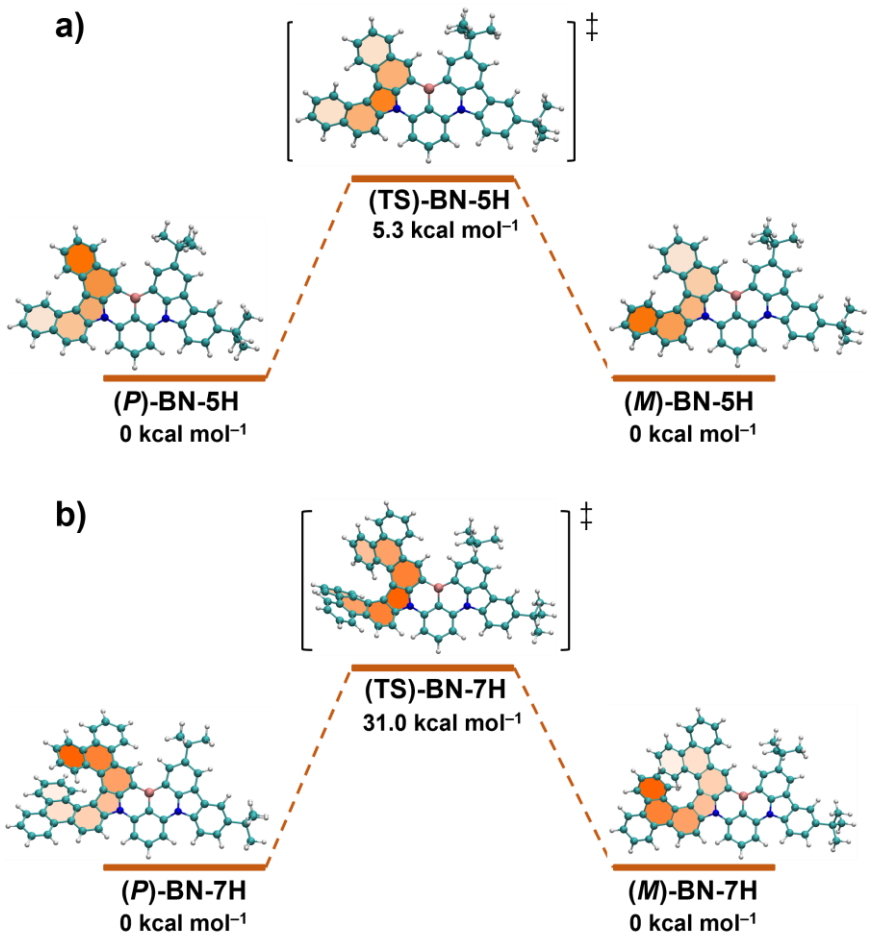


**Figure S26.** Isomerization process from (*P*)- to (*M*)- configuration of (a) BN-5H and (b) BN-7H. The geometries were optimized at the M062X/6-31G(d) level and the relative Gibbs free energy (kcal $mol^{-1}$) were calculated at the M062X/def2TZVP level. BN-7H exhibits higher configurational stability with a racemization barrier of 31.0 kcal $mol^{-1}$, enabling the chiral separation for chiroptical characterizations. By contrast, BN-5H shows a low racemization barrier of only 5.3 kcal $mol^{-1}$, precluding the possibility of chiral separation at room temperature.

**Table S6.** Summary of the chiroptical properties of the representative chiral MR materials.

| Helical chirality | | | | |
|---|---|---|---|---|
| Compound | $\lambda_{CPL}$ (nm) | $\lvert g_{lum} \rvert \times 10^{-3}$ | $B_{CPL}$ ($M^{-1}$ $cm^{-1}$) | Reference |
| **BN-7H** | **524** | **0.7** | **19.0** | **This work** |
| 1a | ~660 | ~1.5 | 28.5 | *J. Am. Chem. Soc.* **2021**, *143*, 17958. |
| 1b | ~684 | ~2.0 | 37.1 | |
| 1c | ~696 | ~1.5 | 40.0 | |
| helicene-BN | ~520 | 2.1 | – | *CCS Chem*. **2022**, *4*, 3463. |
| BN4 | ~520 | ~1.5 | – | *Adv. Mater*. **2022**, *34*, 2105080. |
| BN5 | ~500 | ~1.5 | – | |
| 3-C2 | ~543 | 1.5 | 65 | *Angew. Chem. Int. Ed.* **2023**, *62*, e202218965. |
| 4-C1 | ~520 | 1.1 | 36 | |

| | | | | |
|---|---|---|---|---|
| BN-Py | ~530 | 0.52 | – | *Adv. Mater*. **2023**, *35*, 2305125. |
| o[B-N]$_2$N$_2$ | ~550 | 1.0 | 21.3 | *Sci. China Chem.* **2023**, *66*, 2612. |
| RBNN | ~600 | 1.41 | 20.8 | *Adv. Mater.* **2024**, *36*, 2307420. |
| DB-O | ~450 | 1.4 | 23.5 | *Adv. Mater*. **2024**, *36*, 2308314. |
| DB-S | ~450 | 1.5 | 22.4 | |
| BN[9]H | ~560 | 5.8 | 220.75 | *Angew. Chem. Int. Ed.* **2024**, *63*, e202401835. |
| 3b | ~580 | 5.0 | – | *Angew. Chem. Int. Ed*. **2024**, *63*, e202406497. |
| 4 | ~590 | 5.0 | – | |
| 6 | 660 | 3.0 | – | |
| 2a | ~600 | 2.7 | 41.5 | *Angew. Chem. Int. Ed.* **2024**, *63*, e202414383. |
| 1a | ~700 | 2.9 | 2.0 | |
| 2b | ~600 | 2.5 | 45.8 | |
| 2c | ~590 | 2.7 | 58.7 | |
| 1c | 695 | 5.0 | 4.0 | |
| BN-TP-Icz | ~530 | 0.58 | 8.6 | *Chem. Sci.* **2024**, *15*, 15170. |
| H[6]BN1 | ~470 | 0.51 | 5.30 | *Chem. Eur. J.* **2024**, *30*, e202402257. |
| H[6]BN2 | ~470 | 0.48 | 3.35 | |
| tBuPh-BN | ~490 | 1.5 | 19.3 | *Chem. Sci.* **2024**, *15*, 16917. |
| DPA-tBuPh-BN | ~477 | 0.9 | 8.4 | |
| BN8H | ~520 | 0.75 | – | *Adv. Funct. Mater*. **2025**, e17999. |
| Spiro-3TCzBN | 550 | 0.41 | – | *Chem. Sci.* **2025**, *16*, 11539. |
| BN[8]H-ICz | 525 | 0.24 | 1.2 | *InfoMat* **2025**, *7*, e12652. |
| BN[8]H-BO | 550 | 2.75 | 13.7 | |
| IBN9H | ~530 | 2.29 | 114.08 | *Adv. Opt. Mater*. **2025**, e02776. |
| DBN-*m*ICz | 512 | 2.6 | – | *Adv. Mater.* **2025**, DOI: 10.1002/adma.202511560 |
| 2-C2 | 509 | 1.7 | – | *J. Am. Chem. Soc*. **2024**, *146*, 29782. |
| 2-C1 | 500 | 0.75 | – | |
| 3-C2 | 485 | 2.3 | – | |
| QAO-PhCz | ~460 | 1.1 | – | *Chem. Commun.* **2021**, *57*, 11041. |
| QPO-PhCz | ~550 | 1.6 | – | *J. Mater. Chem. C* **2022**, *10*, 4393. |
| Hel-DiDiKTa | 465 | 0.4 | – | *J. Mater. Chem. C* **2022**, *10*, 4861. |
| Planar chirality | | | | |
| Compound | $\lambda_{CPL}$ (nm) | $\lvert g_{lum}\rvert \times 10^{-3}$ | $B_{CPL}$ ($M^{-1}$ $cm^{-1}$) | Reference |
| Czp-tBuCzB | ~480 | 0.54 | – | *Angew. Chem. Int. Ed.* **2023**, *62*, e202217045. |
| Czp-POAB | ~520 | 0.48 | – | |
| Czp-DiKTa | 507 | 0.4 | – | *Adv. Funct. Mater*. **2024**, *34*, 2402036. |
| m-ICz-N-BN | ~500 | 1.0 | – | *Adv. Funct. Mater.* **2025***, 35,* 2504525. |
| m-prCz-N-BN | ~500 | 1.1 | – | |
| PCP-DBNO | 526 | 1.2 | 35 | *Adv. Mater.* **2025**, DOI: 10.1002/adma.202511230. |
| DpCp-Cz-BN | ~510 | 0.62 | – | *Adv. Optical Mater.* **2025***,* DOI: 10.1002/adom.202502729. |
| DpCp-PXZ-BN | ~500 | 0.42 | – | |

| | | | | |
|---|---|---|---|---|
| DpCp-PTZ-BN | ~500 | 0.41 | – | |
| DpCp-PSeZ-BN | ~500 | 0.40 | – | |
| Axial chirality | | | | |
| Compound | $\lambda_{CPL}$ (nm) | $\lvert g_{lum}\rvert \times 10^{-3}$ | $B_{CPL}$ ($M^{-1}$ $cm^{-1}$) | Reference |
| OBN-2CN-BN | ~500 | 0.91 | – | *Adv. Mater*. **2021**, *33*, 2100652. |
| OBN-4CN-BN | ~510 | 1.04 | – | |
| DOBN | 455 | 1.0 | – | *Adv. Mater.* **2022**, *34*, 2204253. |
| DOBNT | 458 | 0.9 | – | |
| BACzBO | ~500 | 0.73 | – | *Mater. Horiz.* **2024**, *11*, 1752. |
| BA23CzBN | ~510 | 0.35 | – | *Adv. Funct. Mater.* **2024**, *34*, 2403191. |
| BA34CzBN | ~530 | 0.77 | – | |
| BDBF-BOH | ~460 | 0.68 | – | *Angew. Chem. Int. Ed*. **2024**, *63*, e202407277. |
| BDBT-BOH | ~460 | 0.85 | – | |
| BDBF-BNO | 460 | 1.7 | 34.7 | *Adv. Funct. Mater*. **2024**, *34*, 2403803. |
| BDBT-BNO | 460 | 1.8 | 69.1 | |
| DtCzB-OBN | ~500 | 0.386 | 15.76 | *Adv. Opt. Mater*. **2024**, *12*, 2400685. |
| DtCzB-BN | ~500 | 0.774 | 20.40 | |
| S-AX-BN | ~500 | 2.2 | – | *Adv. Funct. Mater.* **2025***, 35,* 2412044. |
| SO2-AX-BN | ~500 | 1.4 | – | |
| BBCz-BN | ~480 | 5.8 | – | *Adv. Funct. Mater.* **2025***, 35,* 2421020. |
| OBBCz-BN | ~490 | 2.5 | – | |
| BIPNX-BN | ~490 | 1.2 | – | *Chem. Eng. J.* **2025***, 505,* 159719. |
| 8*H*-BIPNX-BN | ~500 | 1.8 | – | |
| 8*H*-BIPTZ-BN | ~500 | 0.8 | – | |
| Central chirality | | | | |
| Compound | $\lambda_{CPL}$ (nm) | $\lvert g_{lum}\rvert \times 10^{-3}$ | $B_{CPL}$ ($M^{-1}$ $cm^{-1}$) | Reference |
| Spiro-BNCz | 528 | 1.3 | – | *Aggregate*, **2024**, *5*, e445. |
| p-Spiro-DtBuCzB | 491 | 0.326 | – | *Sci. China Chem.* **2024***, 67,* 2257. |
| m-Spiro-DtBuCzB | 502 | 0.655 | – | |
| NBOPO | ~460 | 1.18 | – | *Mater. Horiz.* **2024***, 11,* 4722. |
| NBNPO | ~500 | 4.30 | – | |
| 2PSFIBN | ~525 | 2.9 | – | *Sci. China Chem.* **2025***, 68,* 4224. |
| 3PSFIBN | ~540 | 4.7 | – | |
| 4PSFIBN | ~530 | 1.9 | – | |
| 2SSFIBN | ~540 | 1.7 | – | |
| 3SSFIBN | ~540 | 5.4 | – | |
| 4SSFIBN | ~520 | 0.7 | – | |
| 4-POtBuCzB | 493 | 0.40 | – | *CCS Chem.* **2025***, 7,* 2419. |
| DWBN | ~450 | 0.5 | – | *Sci. China Chem.* **2025***, 68,* 5795. |

# 8. NMR and HRMS Spectra

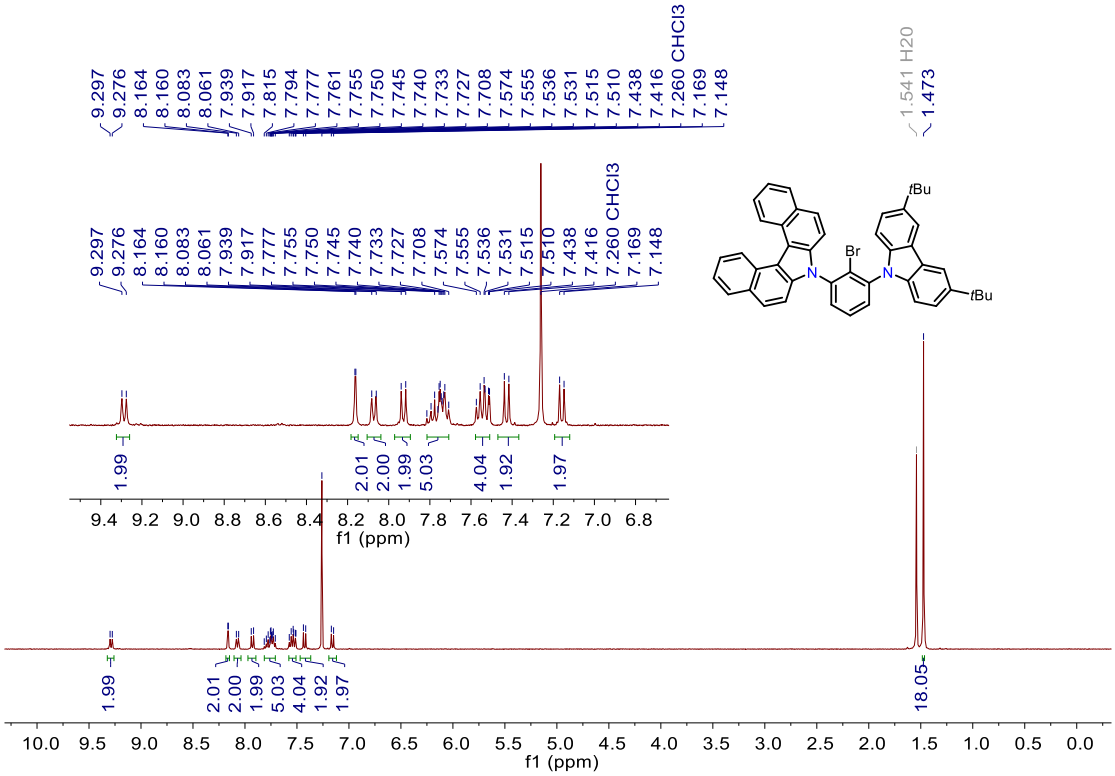


**Figure S27.** $^{1}$H NMR spectrum of **5H-Br** (400 MHz, $CDCl_3$, 297 K).

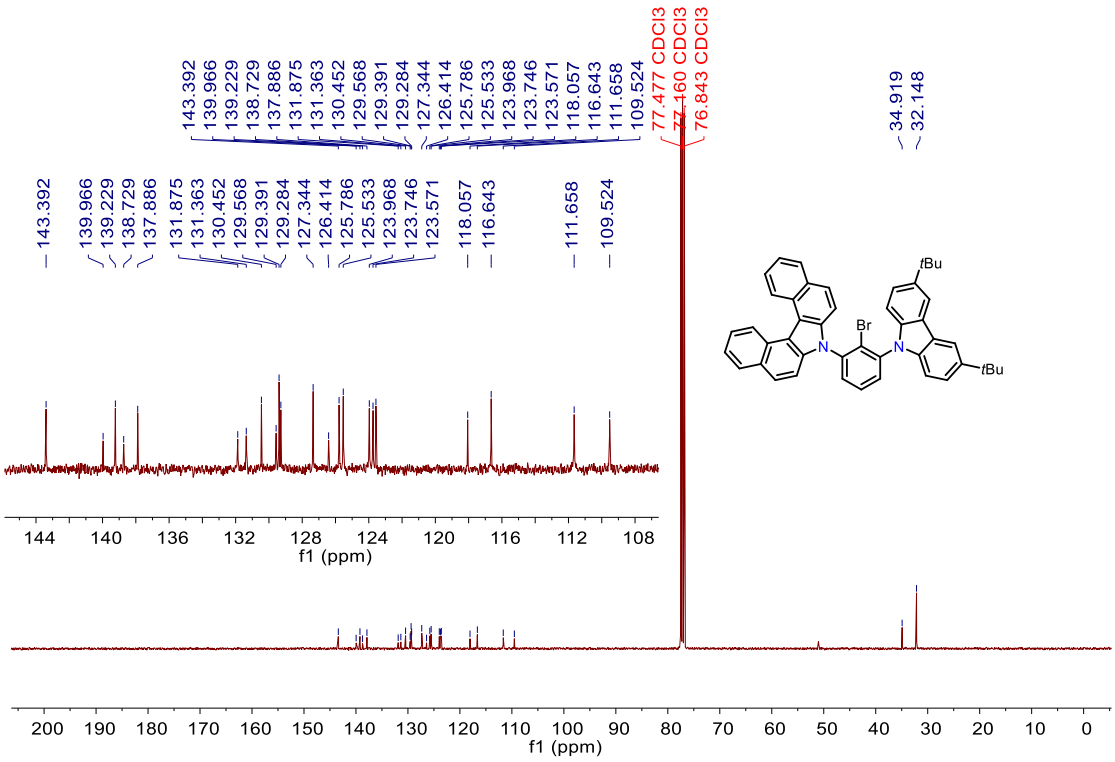


**Figure S28.** $^{13}$C NMR spectrum of **5H-Br** (100 MHz, $CDCl_3$, 297 K).

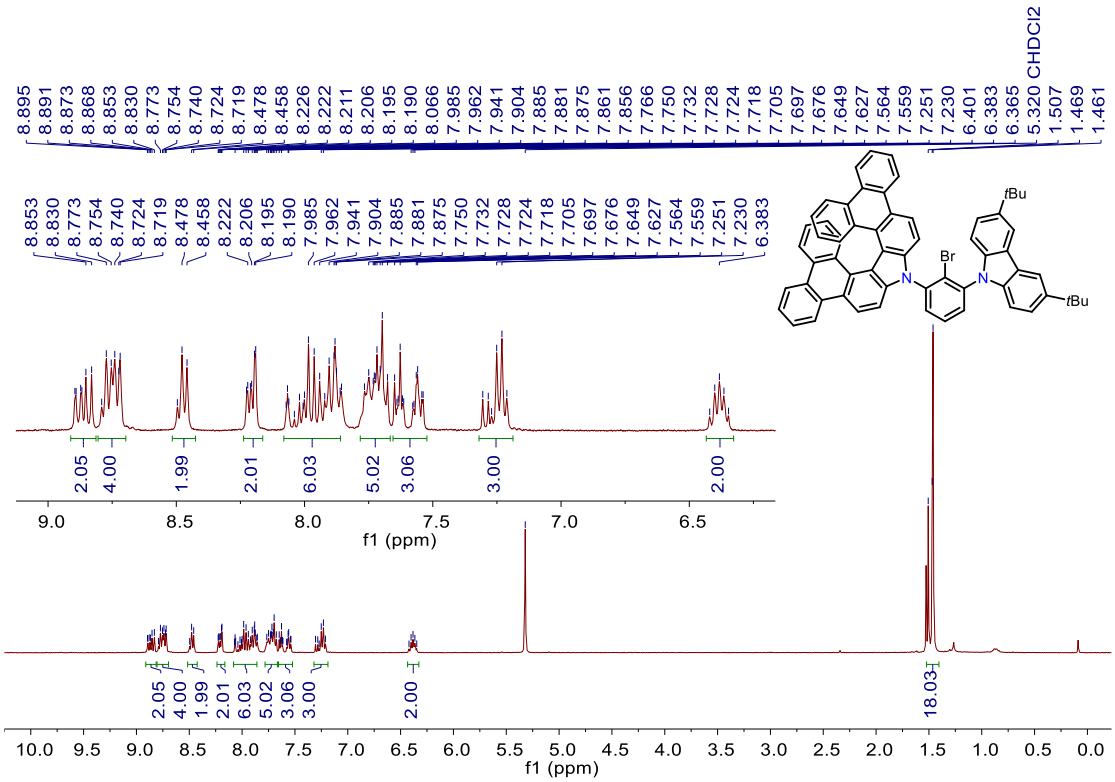


**Figure S29.** $^{1}$H NMR spectrum of **7H-Br** (400 MHz, $CD_2Cl_2$, 297 K).

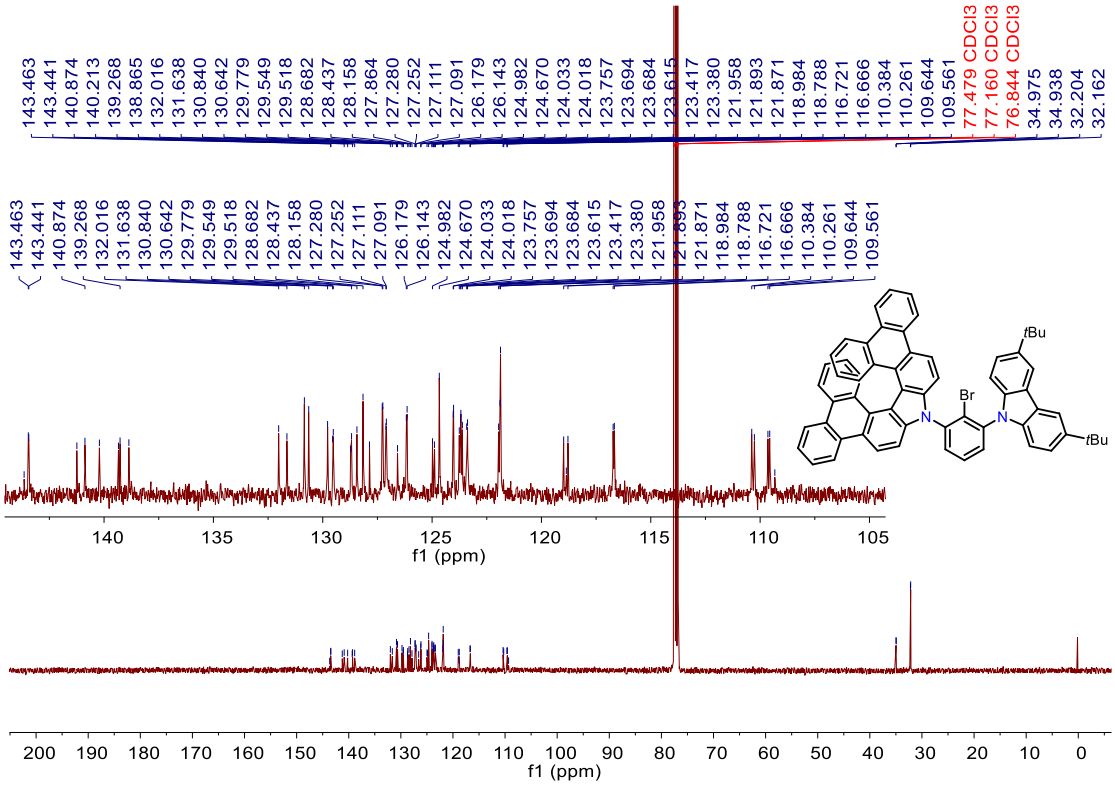


**Figure S30.** $^{13}$C NMR spectrum of **7H-Br** (100 MHz, $CDCl_3$, 297 K).

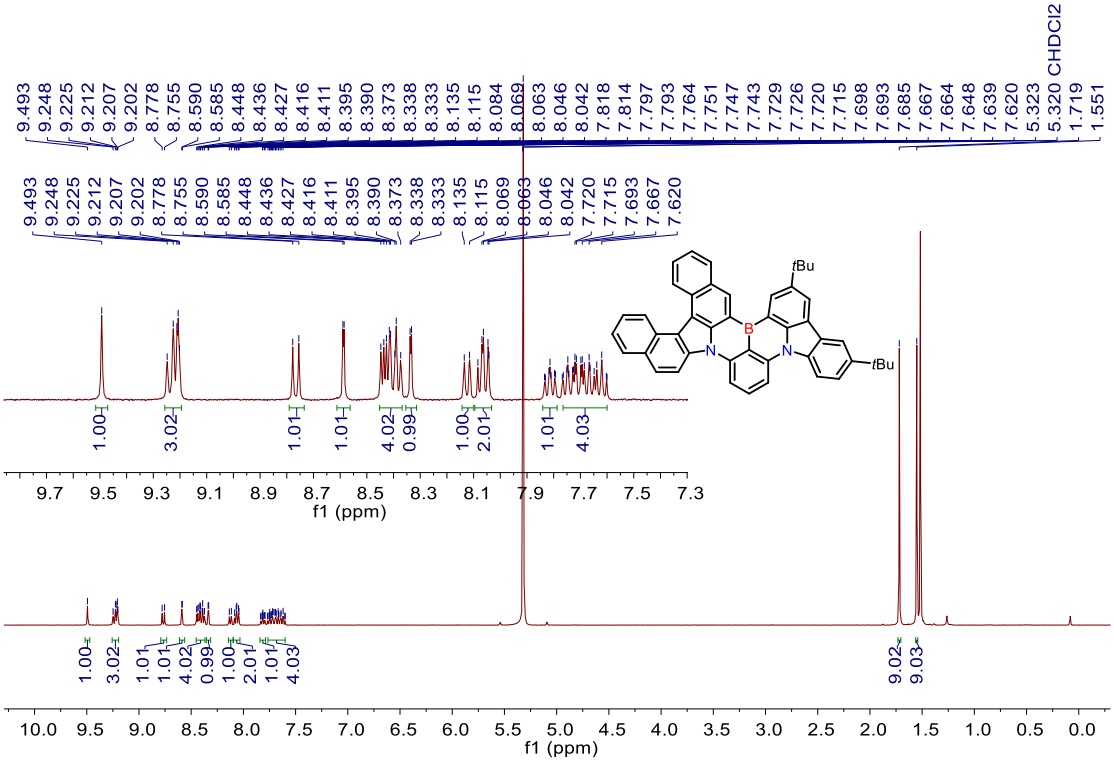


**Figure S31.** $^{1}$H NMR spectrum of **BN-5H** (400 MHz, $CD_2Cl_2$, 297 K).

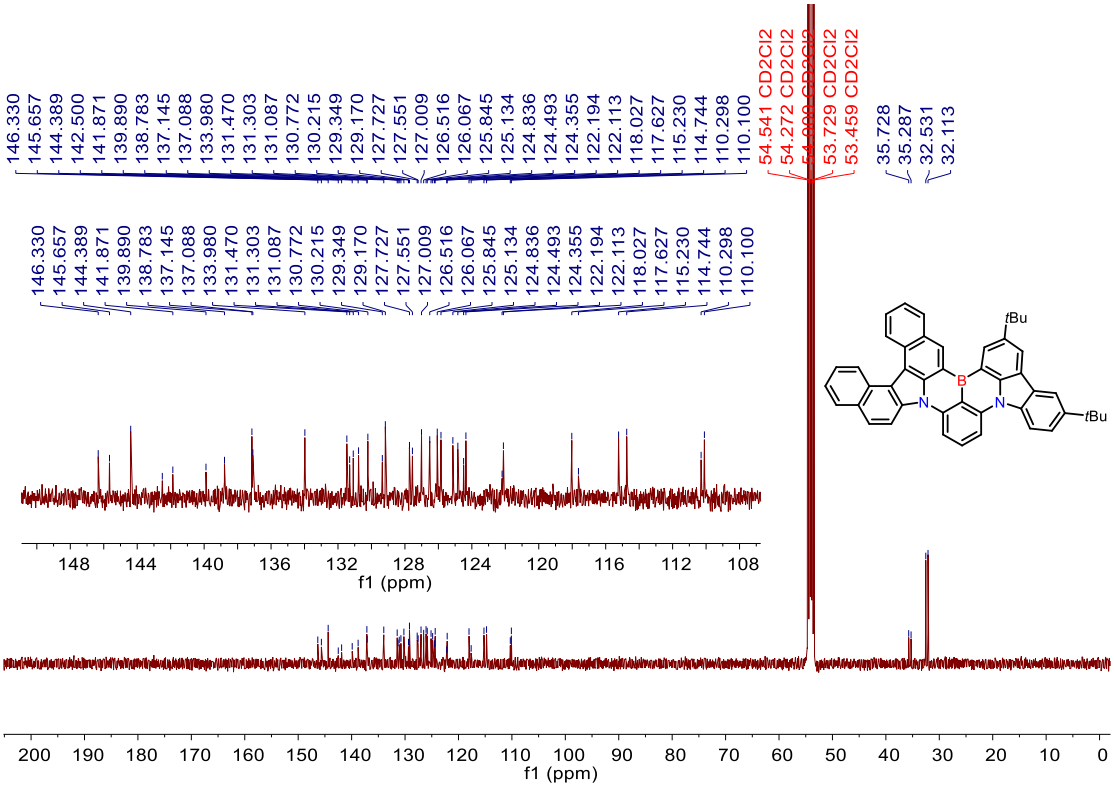


**Figure S32.** $^{13}$C NMR spectrum of **BN-5H** (100 MHz, $CD_2Cl_2$, 297 K).

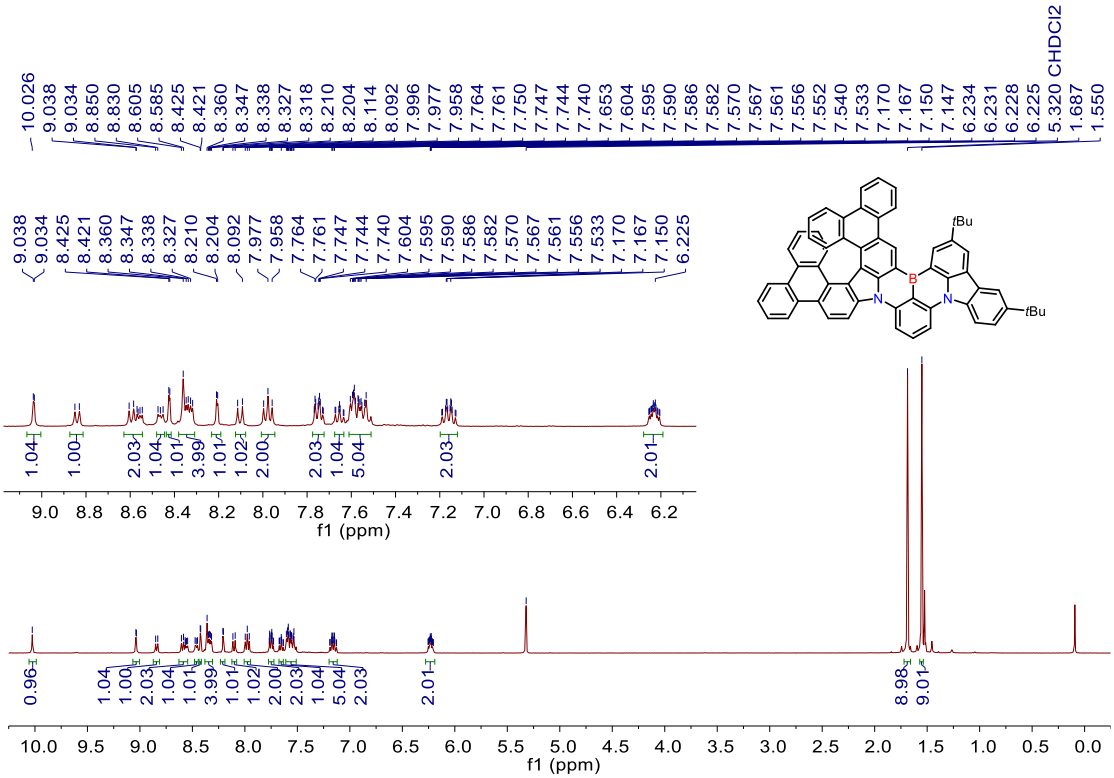


**Figure S33.** $^{1}$H NMR spectrum of **BN-7H** (400 MHz, $CD_2Cl_2$, 297 K).

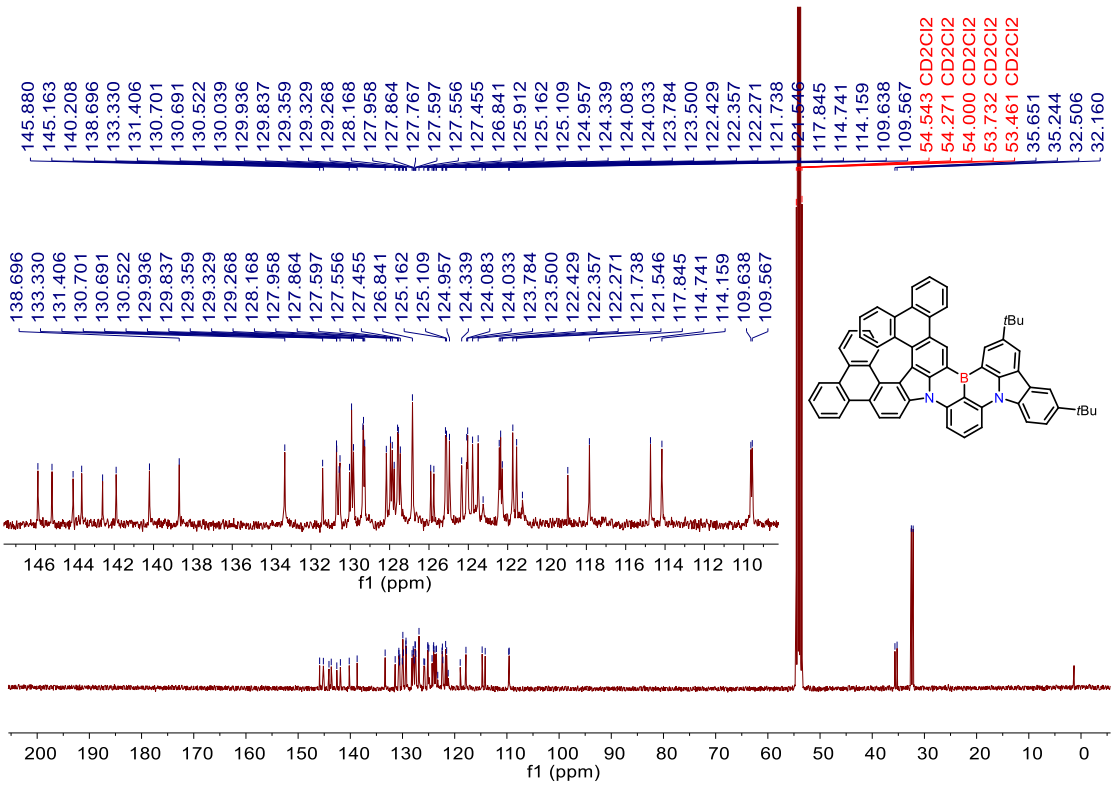


**Figure S34.** $^{13}$C NMR spectrum of **BN-7H** (100 MHz, $CD_2Cl_2$, 297 K).

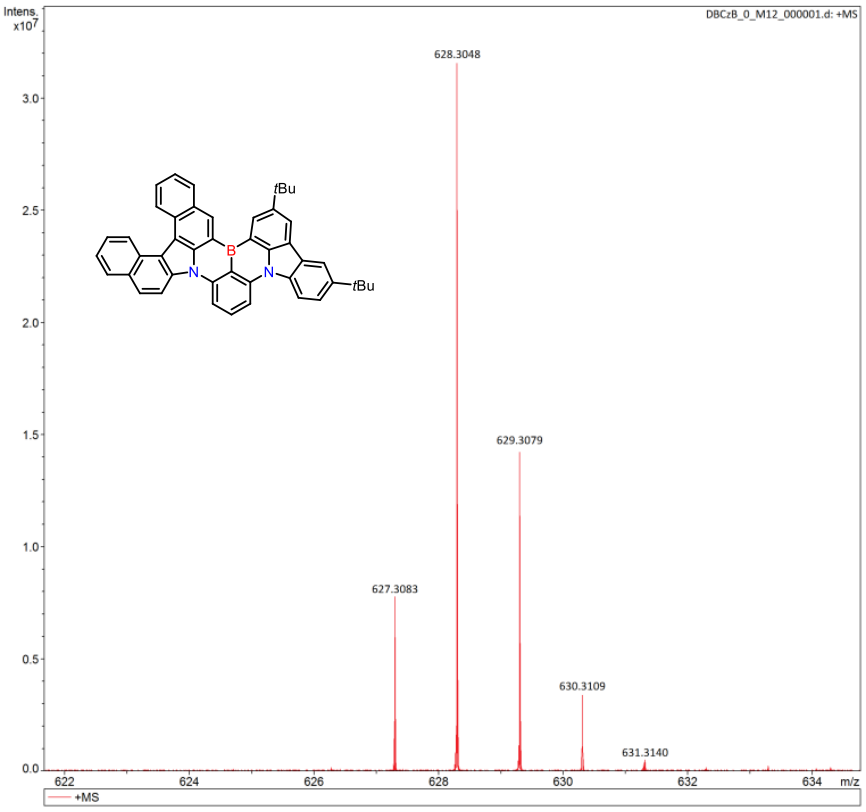


**Figure S35.** High-resolution MALDI-MS spectrum of **BN-5H**.

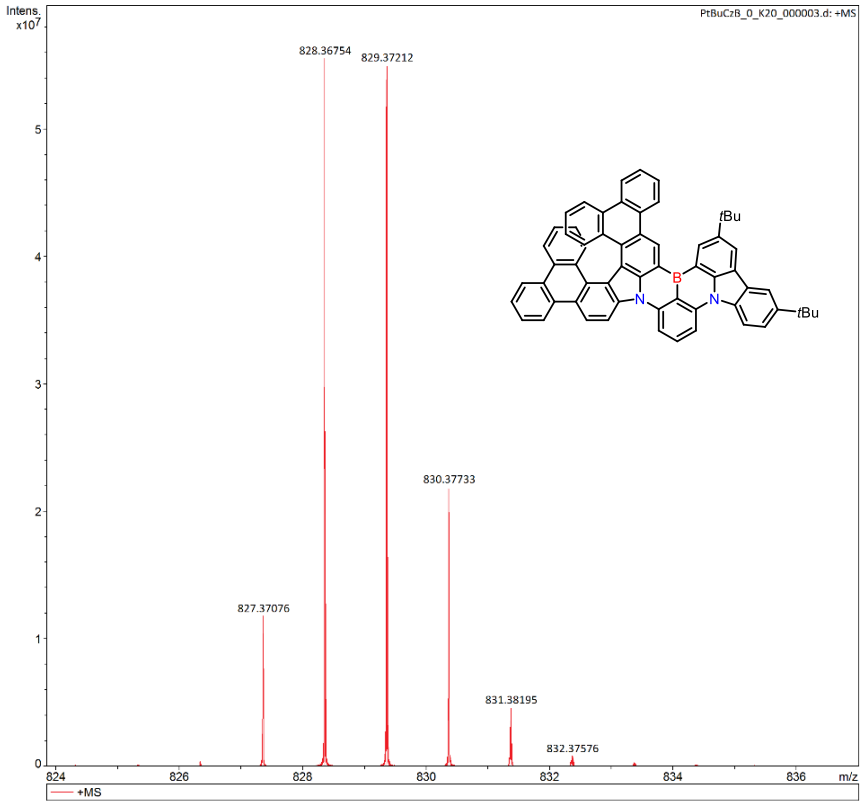


**Figure S36.** High-resolution MALDI-MS spectrum of **BN-7H**.

# 9. References


1 C. Maeda, K. Nagahata, T. Shirakawa and T. Ema, *Angew. Chem. Int. Ed.*, 2020, **59**, 7813−7817.

2 X. Cai, J. Xue, C. Li, B. Liang, A. Ying, Y. Tan, S. Gong and Y. Wang, *Angew. Chem. Int. Ed.*, 2022, **61**, e202200337.

3 M. J. Frisch, G. W. Trucks, H. B. Schlegel, G. E. Scuseria, M. A. Robb, J. R. Cheeseman, G. Scalmani, V. Barone, B. Mennucci, G. A. Petersson, H. Nakatsuji, M. Caricato, X. Li, H. P. Hratchian, A. F. Izmaylov and G. Z. J. Bloino, J. L. Sonnenberg, M. Hada, M. Ehara, K. Toyota, R. Fukuda, J. Hasegawa, M. Ishida, T. Nakajima, Y. Honda, O. Kitao, H. Nakai, T. Vreven, J. A. Montgomery, Jr., J. E. Peralta, F. Ogliaro, M. Bearpark, J. J. Heyd, E. Brothers, K. N. Kudin, V. N. Staroverov, T. Keith, R. Kobayashi, J. Normand, K. Raghavachari, A. Rendell, J. C. Burant, S. S. Iyengar, J. Tomasi, M. Cossi, N. Rega, J. M. Millam, M. Klene, J. E. Knox, J. B. Cross, V. Bakken, C. Adamo, J. Jaramillo, R. Gomperts, R. E. Stratmann, O. Yazyev, A. J. Austin, R. Cammi, C. Pomelli, J. W. Ochterski, R. L. Martin, K. Morokuma, V. G. Zakrzewski, G. A. Voth, P. Salvador, J. J. Dannenberg, S. Dapprich, A. D. Daniels, O. Farkas, J. B. Foresman, J. V. Ortiz, J. Cioslowski, D. J. Fox.

4 T. Lu and F. Chen, *J. Comput. Chem.*, 2012, **33**, 580−592.

5 Z. Liu, T. Lu and Q. Chen, *Carbon*, 2020, **165**, 461-467.

6 W. Humphrey, A. Dalke and K. Schulten, *J. Molec. Graphics.*, 1996, **14**, 33−38.

7 Y. Niu, W. Li, Q. Peng, H. Geng, Y. Yi, L. Wang, G. Nan, D. Wang and Z. Shuai, *Mol. Phys.*, 2018, **116**, 1078−1090.

8 Q. Peng, Y. Yi, Z. Shuai and J. Shao, *J. Am. Chem. Soc.*, 2007, **129**, 9333−9339.

9 Y. Niu, Q. Peng and Z. Shuai, *Sci. China Ser. B-Chem.*, 2008, **51**, 1153−1158.

10 Z. Shuai, *Chin. J. Chem.*, 2020, **38**, 1223−1232.

11 Z. Shuai and Q. Peng, *Phys. Rep.*, 2014, **537**, 123−156.

12 Z. Shuai and Q. Peng, *Nat. Sci. Rev.*, 2017, **4**, 224−239.

13 G. Meng, H. Dai, Q. Wang, J. Zhou, T. Fan, X. Zeng, X. Wang, Y. Zhang, D. Yang, D. Ma, D. Zhang and L. Duan, *Nat. Commun.*, 2023, **14**, 2394.

14 Z. Yang, Z. Mao, Z. Xie, Y. Zhang, S. Liu, J. Zhao, J. Xu, Z. Chi and M. P. Aldred, *Chem. Soc. Rev.*, 2017, **46**, 915-1016.

15 T. Huang, Q. Wang, S. Xiao, D. Zhang, Y. Zhang, C. Yin, D. Yang, D. Ma, Z. Wang and L. Duan, *Angew. Chem. Int. Ed.*, 2021, **60**, 23771−23776.